DOI: 10.1002/cmdc.201402394

Targeting Promoter G-Quadruplex DNAs by Indenopyrimidine-Based Ligands

K. V. Diveshkumar, Saaz Sakrikar, S. Harikrishna, V. Dhamodharan, and P. I. Pradeepkumar*[a]

The formation of G-quadruplex structures can regulate telomerase activity and the expression of oncogenes at the transcriptional and translational levels. Therefore, stabilization of G-quadruplex DNA structures by small molecules has been recognized as a promising strategy for anticancer drug therapy. One of the major challenges in this field is to impart stabilizing molecules with selectivity toward quadruplex structures over duplex DNAs, and to maintain specificity toward a particular quadruplex topology. Herein we report the synthesis and binding interactions of indenopyrimidine derivatives, endowed with drug-like properties, with oncogenic promoters of *c-myc* and *c-kit*, telomeric and duplex DNAs. The results show specific stabilization of promoter over telomeric quadruplexes and duplex DNAs. Molecular modeling studies support the experimental observations by unraveling the dual binding mode of ligands by exploiting the top and bottom quartets of a G-quadruplex structure. This study underscores the potential of the indenopyrimidine scaffold, which can be used to achieve specific G-quadruplex-mediated anticancer activity.

Introduction

G-quadruplexes are four-stranded secondary nucleic acid structures formed by guanine-rich sequences. Potential quadruplex-forming sequences are found in telomeres (chromosomal ends), promoter regions of oncogenes, introns and UTRs of mRNAs.[1–3] Human telomeric repeat sequences are able to fold into quadruplex structures with various topologies such as antiparallel, hybrid, and parallel under physiological conditions (Figure 1).[2] Stabilization of these quadruplex structures by small molecules has been shown to inhibit telomerase activity, thereby halting cancer progression.[2] The promoter regions of important proto-oncogenes such as *c-myc*, *c-kit*, *vegf*, *bcl-2*, and *hif-1α* contain G-rich sequences, which have a propensity to form parallel quadruplex structures.[4–6] Unlike telomeric DNA, promoter quadruplex-forming sequences, being present in the double-stranded form, must compete energetically with duplex DNA to form quadruplex structures. However, molecular crowding conditions and dynamic forces derived from negative superhelicity aid in the formation of promoter quadruplex structures.[7] Proto-oncogenes such as *c-myc* and *c-kit* are overexpressed up to 80% in various tumors such as gastrointestinal, ovarian, and breast cancers.[6] The promoter region of *c-myc* DNA contains seven nuclease-hypersensitive elements (NHEs), in which NHE III_1, located from −142 to −115 base pairs upstream of the P_1 promoter, contains quadruplex-forming sequences. Since the NHE III_1 region controls 90% of *c-myc* expression, stabilization of G-quadruplex structures by small molecules in this region can regulate gene expression.[8,9] Another widely studied proto-oncogene is *c-kit*, which plays an important role in cell survival, proliferation, and differentiation.[6] Two quadruplex-forming sequences, namely *c-kit1* and *c-kit2*, are present in the same core promoter: *c-kit1* DNA between −87 and −109 base pairs, and *c-kit2* DNA between −140 and −160 base pairs from the transcription start site.[10] The use of small molecules to stabilize G-quadruplex structures present in *c-kit* DNAs can regulate gene expression and thus inhibit a wide range of cancerous growths.[5]

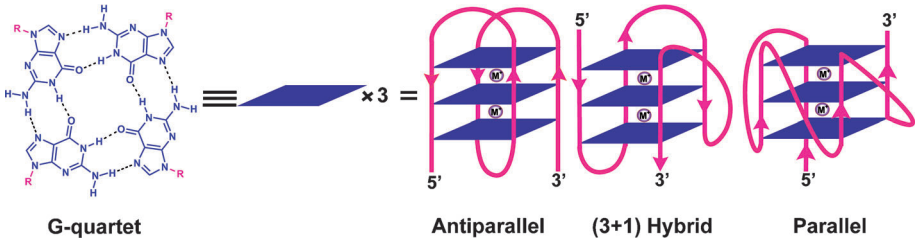

Figure 1. Schematic representation of a G-quartet and various quadruplex structural motifs. The G-quartet is formed by self-association of guanine bases through Hoogsteen hydrogen bonding; formation of the G-quadruplex structure occurs through stacking of G-quartets stabilized by monovalent metal ions.

The structure, stability, and topology of G-quadruplex DNAs depend on various factors such as the nature of metal ions present, as well as the sequence and length of the loops.[1–3]

[a] *K. V. Diveshkumar, S. Sakrikar, S. Harikrishna, V. Dhamodharan, Prof. P. I. Pradeepkumar*
Department of Chemistry
Indian Institute of Technology Bombay, Powai, Mumbai 400076 (India)
E-mail: pradeep@chem.iitb.ac.in

Supporting information for this article is available on the WWW under http://dx.doi.org/10.1002/cmdc.201402394.

Monovalent cations such as K^+ and Na^+ can stabilize the quadruplex structure by neutralizing the negative potential created by oxygen atoms of guanine bases.[11] G-quadruplex structures can be formed from a single strand (intramolecular) or multiple strands (intermolecular), and the topology can be parallel, antiparallel, or mixed-hybrid type, depending on the nature of the loops (Figure 1).[12] Therefore, the major challenge in targeting G-quadruplexes lies in the design of small molecules that can selectively stabilize quadruplexes over various DNA structures and achieve specificity among various quadruplex topologies.

A large number of molecules have been explored for their selective stabilization of quadruplex DNAs over duplex DNAs.[13–18] TMPyP4, a porphyrin derivative, is a well-studied quadruplex stabilizer both in vitro and in vivo and shows anticancer activity.[19] The ligand was found to be nonselective, as it showed affinity for other DNA structures including duplex DNAs. However, the selectivity toward quadruplex DNAs was later improved through various TMPyP4 derivatives such as metallated and phenol quaternary ammonium porphyrins.[20,21] Telomestatin and its derivatives,[22] acridine derivatives,[23] perylene,[24] quarfloxin,[25] and corolone derivatives[26] were reported for their selective stabilization of telomeric quadruplexes over duplex DNAs. Triazole-linked acridine derivatives have been reported for their selective binding of telomeric quadruplex DNAs over duplex and *c-kit* quadruplex DNAs.[27] An acyclic telomestatin heptamer derivative, TOxaPy, was reported for its potency in recognizing antiparallel topology (under Na^+ conditions) over the mixed-hybrid topology (under K^+ conditions) of telomeric quadruplex DNAs.[28] Although the molecule showed selectivity over duplex DNAs, moderate stabilization was obtained with *c-myc* and *c-kit* promoter quadruplex DNAs having parallel topology.[28] Conversely, *N*-methyl mesoporphyrin IX (NMM) was reported for its ability to induce and stabilize a parallel topology of telomeric quadruplex DNAs under K^+ conditions over antiparallel (under Na^+ conditions) telomeric quadruplex DNAs.[29,30] Ellipticine derivatives,[31] piperazinyl-substituted quindolines,[32] bisindole carboxamide derivatives,[33] diethynyl pyridine derivatives,[34] and furan-based oligopeptides[35] were also reported for their preferential affinity for promoter quadruplexes over duplex DNAs. A recent study from our research group has reported bisquinolium and bispyridinium derivatives of naphthyridine, which can selectively stabilize telomeric and promoter quadruplex DNAs over duplex DNAs.[36,37] Notably, most of the small molecules reported thus far have limited preference for a given topology, or lack drug-like properties.

The wealth of structural information on promoter quadruplexes shows that most of the promoter quadruplexes adopt parallel topology and have unique grooves and loops (medium-sized grooves and propeller loops).[12] Therefore, specific stabilization of such parallel promoter quadruplexes can be achieved by small molecules, which are designed to interact with grooves or loops along with top and bottom quartets of G-quadruplex structures. Along these lines, we report herein three derivatives of indenopyrimidine that are capable of specifically stabilizing the promoter quadruplex DNAs over human telomeric and duplex DNAs (Figure 2). A detailed evaluation of the specific stabilization properties toward promoter quadruplex DNAs by these molecules was carried out using various biophysical methods (CD titration, CD melting, fluorimetric titrations, Job plot analysis) biochemical assays (*Taq* DNA polymerase stop assays), molecular modeling, and dynamics studies.

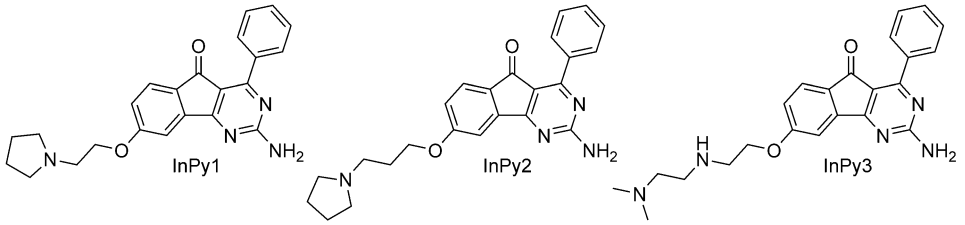

Figure 2. Structures of DNA G-quadruplex-stabilizing ligands. Ligands **InPy1** and **InPy2** contain pyrrolidine side chains of varying length, whereas **InPy3** has an *N*,*N*-dimethylethane side chain; all three contain the same aryl indenopyrimidine core.

Results and Discussion

Ligand design and synthesis

Indenopyrimidine derivatives were previously reported as antagonists of dual A_{2A}/A_1 adenosine receptors for the potential treatment of Parkinson's disease.[38] Several derivatives of indenopyrimidine were demonstrated to have potent activity in animal models of Parkinson's disease.[38] We hypothesized that aryl indenopyrimidine derivatives can be tuned as efficient G-quadruplex-stabilizing ligands owing to their simplicity in structure, synthesis, and drug-like properties. We designed and synthesized three derivatives of indenopyrimidine that can satisfy the structural features of G-quadruplex-stabilizing agents (Figure 2). These compounds contain an aromatic core that can stack on the G-quartet, and ethyl/propyl side chains terminated with an amino functionality, which will aid interaction with the negatively charged phosphate backbone of the grooves and loops of quadruplex structures. Moreover, low molecular weight and a minimal number (less than five) of hydrogen bond acceptors and donors contribute to the drug-like properties of these molecules.

Synthetic access to the indenopyrimidine derivatives is depicted in Scheme 1. All three derivatives (**InPy1**–**3**) were synthesized from commercially available starting materials 6-methoxyindanone (**1**) and benzaldehyde (**2**). Preparation of the intermediate compound **5** was carried out by following reported procedures with slight modifications.[38] Compound **1** was condensed with **2** under acidic conditions to obtain **3** in 85% yield. Dehydrated aldol product **3** was first refluxed with free

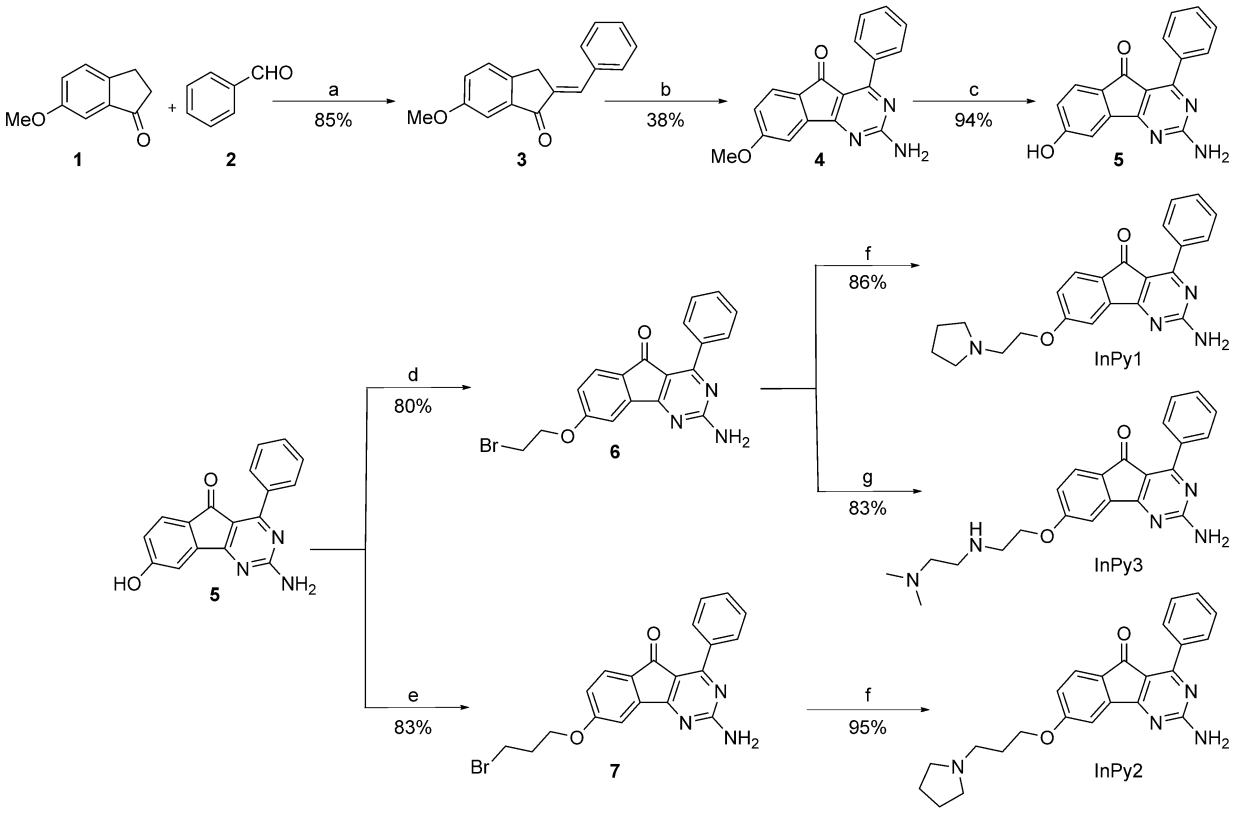

Scheme 1. Synthesis of indenopyrimidine derivatives **InPy1**, **InPy2**, and **InPy3**. *Reagents and conditions*: a) AcOH, conc HCl, 90 °C, 6 h; b) 1. guanidine·HCl, NaOH, EtOH, 80 °C, 18 h, 2. air, NaOH, DMF, 80 °C, 16 h; c) LiCl, H_2O, NMP, 180 °C, 62 h; d) 1,2-dibromoethane, K_2CO_3, CH_3CN, 75 °C, 18 h; e) 1,3-dibromopropane, K_2CO_3, CH_3CN, 75 °C, 18 h; f) pyrrolidine, CH_3CN, reflux, 3 h; g) *N*,*N*-dimethylethane-1,2-diamine, CH_3CN, reflux, 3 h.

guanidine base (obtained by treating guanidine hydrochloride with sodium hydroxide), which, upon further oxidation in air, furnished the cyclized product **4** in 38% yield. Hydrolysis of **4** with lithium chloride and water in *N*-methyl-2-pyrrolidone afforded compound **5** in 94% yield.[38] Treatment of compound **5** with 1,2-dibromoethane and 1,3-dibromopropane under basic conditions delivered compounds **6** and **7** in respective yields of 80 and 83%.[39] Finally, **6** was refluxed with pyrrolidine and *N*,*N*-dimethylethane-1,2-diamine to afford the final compounds **InPy1** and **InPy3** in 86 and 83% yields, respectively. Similarly, compound **7** was refluxed with pyrrolidine to furnish **InPy2** in 95% yield.

Circular dichroism studies

Circular dichroism (CD) spectroscopy is a practical tool to gain insight into various topologies, the effects of metal ions, and the stability G-quadruplex structures.[40] Although CD spectroscopy does not account for the molecularity (intra versus inter) of the DNA strands involved in forming a quadruplex structure, the potential of the ligands to induce and stabilize various quadruplex topologies can be well studied by CD titration experiments. In CD spectra, positive peaks at 290 and 240 nm, and a negative peak at 260 nm represent an antiparallel quadruplex structure, whereas a dominant positive peak at 260 and a negative peak at 240 nm reflect parallel quadruplex topology.[34,41,42]

The interactions of ligands with telomeric and promoter quadruplex DNAs, *c-myc* and *c-kit1*, in the presence and absence of added metal ions were studied by CD titration experiments. Titration of the human telomeric DNA with **InPy1** in the absence of added monovalent cations was carried out to explore the capacity of the ligand to induce a particular quadruplex topology. CD spectra of telomeric DNA without ligands exhibited a small positive peak at 255 and a negative peak at 234 nm, which do not account for any particular quadruplex topology (Figure 3 A). However, titration with **InPy1** resulted in decreased ellipticity for the peaks at 255 and 234 nm. At higher ligand concentration, the appearance of a new peak around 295 nm was observed, which cannot be attributed to any quadruplex topology. These results clearly show that **InPy1** is incapable of inducing any particular quadruplex topology in telomeric DNA. However, in the case of **InPy2** and **InPy3**, weak enhancement of peaks at 290 and 260 nm were observed at higher ligand concentrations, indicating weak induction of antiparallel topology for telomeric DNA (Figure S1, Supporting Information). Titration of telomeric DNA under added K^+ conditions showed a strong peak around 290 nm along with a shoulder peak around 255 nm and a small peak around 235 nm that are characteristic peaks for a (3 + 1) hybrid quadruplex structure (Figure S1, Supporting Information).[41]

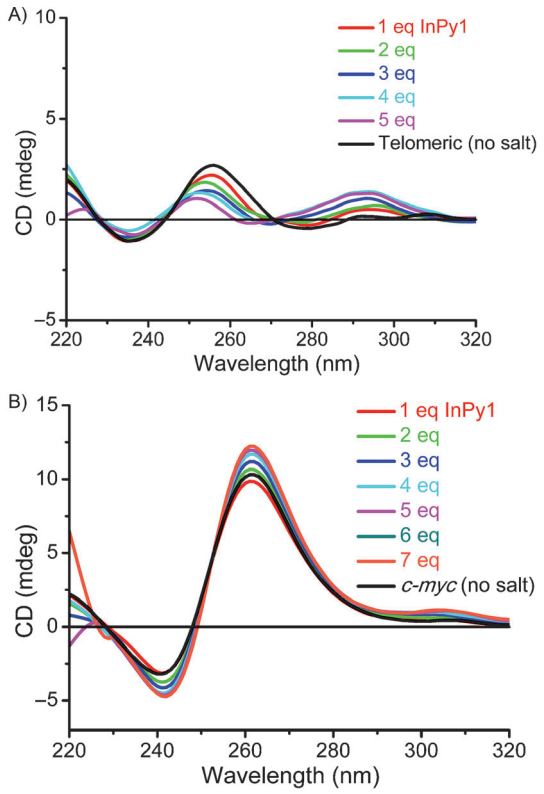

Figure 3. CD titration spectra of A) telomeric and B) wild-type *c-myc* DNA with **InPy1** in the absence of added metal ions (12.5 μM DNA in 50 mM Tris, pH 7.2).

There was no further significant change in the spectra observed upon titration with increasing concentrations of **InPy1** (0–5 equiv), indicating the absence of any conformational changes and retention of the pre-folded quadruplex structure. Additionally, no significant changes in the CD spectra were observed by titrating telomeric DNA with **InPy1** in the presence of added Na^+ ions, indicating retention of the existing antiparallel topology (Figure S1, Supporting Information).[42]

Promoter quadruplex DNAs were reported for their ability to form a strong parallel topology even in the absence of added monovalent cations.[34] CD titration experiments for *c-myc* and *c-kit1* in the presence and absence of added monovalent ions were performed with increasing concentrations of ligands to study their ability to induce or enhance conformational changes in the existing quadruplex topology. CD spectra of *c-myc* and *c-kit1* in the absence of added K^+ ions showed an increase in ellipticity of peaks at 260 and 240 nm, clearly indicating further induction of existing parallel quadruplex topology (Figure 3B and Figures S2 and S3, Supporting Information). CD spectra for *c-myc* and *c-kit1* DNAs in the presence of added K^+ ions clearly showed the presence of parallel topology, and upon titration with ligands **InPy1**, **InPy2**, and **InPy3**, retention of the existing parallel topologies was observed (Figures S2 and S3, Supporting Information). It was evident from the CD titration experiments that all ligands are able to further induce and stabilize existing parallel topology in promoter quadruplex DNAs.

CD melting studies

Thermal stabilization properties of ligands with quadruplex and duplex DNAs can be studied with the aid of CD spectroscopy by comparing the melting temperatures of DNAs at a suitable wavelength in the presence or absence of ligands.[43] For telomeric DNA, melting studies were performed under K^+ (mixed-hybrid topology) and under Na^+ conditions (antiparallel topology) by monitoring ellipticity at 295 nm. Telomeric DNA in the absence of ligands showed T_m values of 54 and 45 °C under K^+ and Na^+ conditions, respectively (Figure 4A,

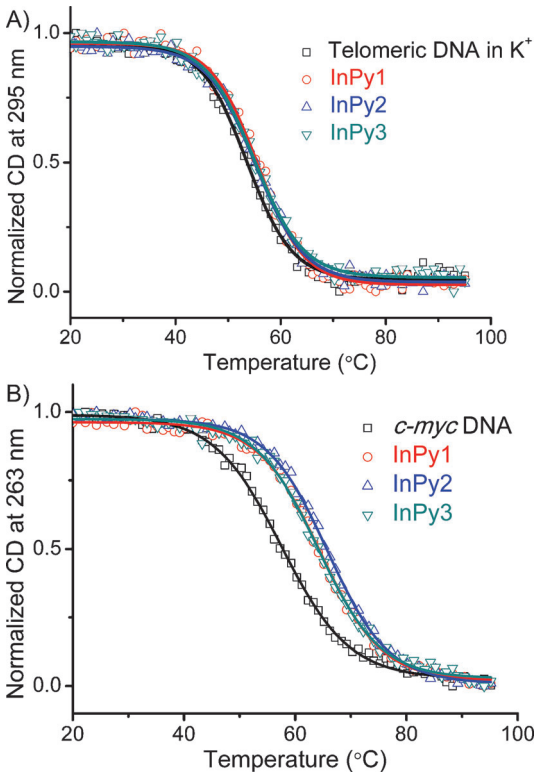

Figure 4. CD melting curves for A) telomeric [10 mM KCl, 90 mM LiCl] and B) *c-myc* [1 mM KCl and 99 mM LiCl] DNAs (10 μM DNA, 10 mM lithium cacodylate buffer, pH 7.2) in the absence or presence of ligands (5 equiv).

and Figure S4, Supporting Information). Strikingly, there was no significant change (maximum $\Delta T_m = 1.5$ °C) in the melting temperature under both salt conditions (K^+ and Na^+) for the telomeric quadruplex DNA upon addition of 5 equivalents of the ligands (Table 1). This further validates that ligands do not stabilize telomeric quadruplex DNAs. To determine the selectivity of ligands over duplex DNAs, CD melting studies for duplex DNAs were carried out at 242 nm under similar salt and buffer conditions. Thermal stabilization was very low in the case of duplex DNAs (maximum $\Delta T_m = 0.6$ °C) with any of the ligands, even at higher concentrations (Figure S4, Supporting Information).

The stabilization properties of ligands with promoter *c-myc* and *c-kit1* quadruplex DNAs were monitored at 263 nm under K^+ conditions (Figure 4B, and Figure S4, Supporting Informa-

Table 1. Thermal stability of quadruplex and duplex DNAs with ligands measured by CD melting experiments.

Ligand	ΔT_m [°C][a]				
	c-myc	*c-kit1*	Telomeric (K^+)	Telomeric (Na^+)	Duplex (17 mer)
InPy1	7.8±0.5	9.6±0.5	1.5±0.2	1.2±0.1	0.6±0.2
InPy2	8.2±0.5	10.1±0.2	1.2±0.2	1.1±0.2	0
InPy3	6.6±0.5	9.5±0.2	0.8±0.3	0.2±0.2	0

[a] ΔT_m values are the difference in thermal melting [$\Delta T_m = T_m$(DNA + 5 mol. equiv ligand) − T_m(DNA)] and are reported as the average ± SD of three independent experiments.

tion). For *c-myc* and *c-kit1* quadruplex DNAs in the absence of ligands, the respective melting temperatures were 58 and 44 °C. Interestingly, all three ligands showed higher thermal stabilization with promoter quadruplex DNAs (Table 1). **InPy1** and **InPy2** elicited an increase in the melting temperature (ΔT_m = 7.8–8.2 °C), whereas **InPy3** showed only a moderate increase in melting temperature (ΔT_m = 6.6 °C). Similarly, for *c-kit1* quadruplex DNA, all ligands were able to impart higher stabilization, as evident from their melting temperature (ΔT_m = 10 °C). Thus the results from CD melting studies validate the specific stabilization of promoter quadruplex DNAs over telomeric and duplex DNAs by the ligands.

Fluorescence titration experiments

Fluorescence spectroscopy was used to explore the binding properties of ligands with various quadruplex and duplex DNAs.[44,45] Interaction of ligands with quadruplex DNAs results in either enhancement or quenching of the fluorescence intensity of the ligands. A concentration-dependent increase or decrease in fluorescence intensity can be used to derive the binding constant and stoichiometry for the ligand–quadruplex interaction. Emission spectra for ligand **InPy1** was characterized by an intense peak at 536 nm and a less-intense peak at 414 nm after excitation at 350 nm (Figure 5 A). Fluorimetric titration with increasing concentration of pre-annealed *c-myc* DNA resulted in the quenching of ligand fluorescence together with a blue shift by 20 nm for the peak at 536 nm (Figure 5 A). Quenching of fluorescence upon titration and the blue shift indicate strong binding interactions between the ligand and DNA. Fluorescence intensity was plotted against DNA concentration, and was fitted by using the standard Stern–Volmer equation to derive the binding constant: $K_a = 1.0 \times 10^5\ M^{-1}$ for the ligand **InPy1** (Figure 5 B).[46] Similar titration experiments performed with telomeric and duplex DNAs yield binding constants $K_a = (2.8 \pm 0.3) \times 10^4\ M^{-1}$ and $K_a = (3.6 \pm 0.1) \times 10^4\ M^{-1}$, respectively (Figure S5, Supporting Information).

Similarly, binding constants for *c-myc* ($K_a = 1.6 \times 10^5\ M^{-1}$), telomeric DNA [$K_a = (4.5 \pm 0.4) \times 10^4\ M^{-1}$], and duplex DNA [$K_a = (4.5 \pm 0.1) \times 10^4\ M^{-1}$] were obtained with the ligand **InPy2** (Figure S6, Supporting Information). Binding constant values obtained for *c-myc* quadruplex DNA, together with the observed spectral changes are similar to the reported values for strong ligand–quadruplex interactions.[47–49] The threefold difference in the binding constants observed between *c-myc* and telomeric/duplex DNAs further explains the specificity and selectivity of the ligands.

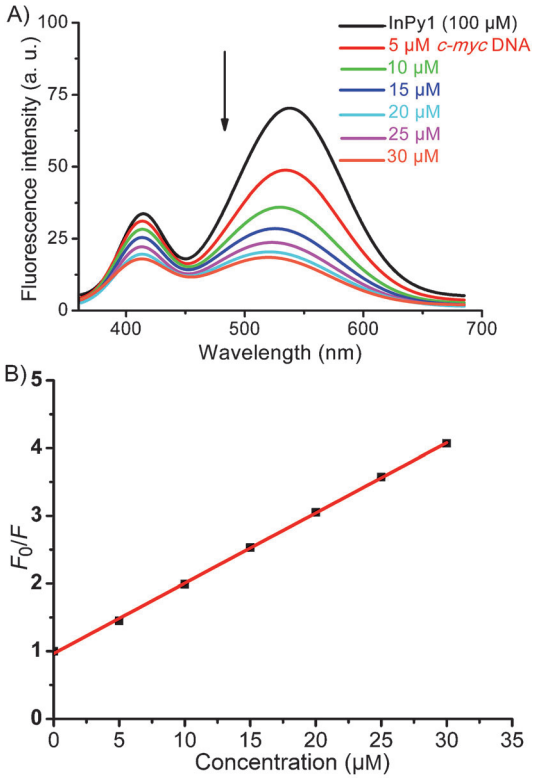

Figure 5. Fluorescence quenching curves and Stern–Volmer plots for **InPy1** with increasing concentrations of *c-myc* DNA. A) **InPy1** (100 μM in 100 mM KCl, 10 mM lithium cacodylate buffer, pH 7.2) with *c-myc* DNA (0–30 μM under identical salt and buffer conditions). B) Stern–Volmer plot for **InPy1** with *c-myc* DNA.

To gain further insight into the binding stoichiometry for the ligand–quadruplex interaction, continuous variation analysis (Job plot) was performed by using the fluorescence properties of **InPy1**.[50] The plot of fluorescence intensity versus mole fraction of the ligand showed a stoichiometry of ~2:1 (ligand/DNA) with *c-myc* quadruplex DNA (Figure S7, Supporting Information). This dual binding mode was further validated by molecular modeling and dynamics studies (see below).

Taq DNA polymerase stop assays

Selective stabilization of promoter quadruplex DNAs by ligands was further explored by concentration-dependent *Taq* DNA polymerase stop assays using *c-myc* and telomeric quadruplex-forming sequences. This assay was carried out by following reported procedures with slight modifications.[51] Templates containing wild-type *c-myc*, mutated *c-myc*, and telomeric quadruplex-forming sequences were used for the primer-extension reaction. Reactions were carried out at 50 °C for *c-myc* and at 40 °C for telomeric DNA to unwind the preformed quadruplex structure. In the case of *c-myc*, a control experiment with template containing a mutated *c-myc* sequence that cannot form

a quadruplex structure was also carried out. If ligands can stabilize the quadruplex structure in the template sequence, primer extension by *Taq* polymerase will be stopped at the quadruplex-forming site. The concentration of ligand required for the formation of 50% stop product would yield an IC_{50} value for the ligands; lower IC_{50} values reflect greater ligand potency. Because the ligands **InPy1** and **InPy2** showed higher thermal stabilization with *c-myc* DNA in CD melting studies, these ligands were selected for the study. In the case of the *c-myc* template, formation of stop products was observed upon increasing ligand concentration (Figure 6A, and Figure S8, Supporting Information). Ligand **InPy1** exhibited 50% inhibition at a concentration of ~46 μM and **InPy2** showed 50% stop product at ~31 μM (Figure S8, Supporting Information). However, stop products were not observed for the mutated *c-myc* template under identical reaction conditions, supporting the fact that stabilization of a quadruplex structure is responsible for the formation of stop products (Figure 6A). In the case of telomeric DNA, a much smaller quantity of stop products (~10%) was obtained, even at the higher ligand concentrations used (up to 160 μM; Figure 6B). The results obtained from the *Taq* DNA polymerase stop assays support the observations from the CD melting experiments, that the ligands are able to stabilize the parallel quadruplex structures present in the promoter DNAs and are unable to stabilize the quadruplex topologies of telomeric DNA.

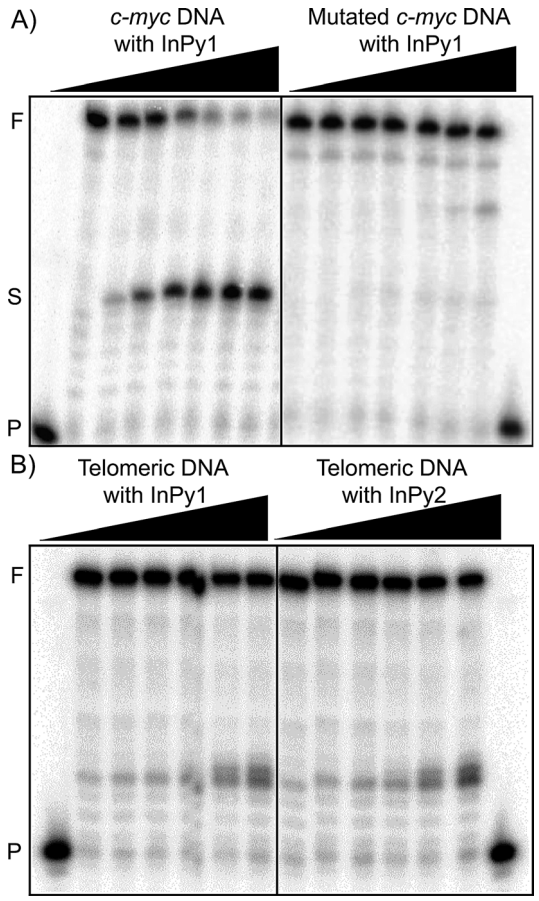

Figure 6. Denaturing PAGE (15%, 7 M urea) of the *Taq* DNA polymerase stop assay in the presence of *c-myc*, mutated *c-myc*, and telomeric DNA with increasing ligand concentrations. A) **InPy1** (0–160 μM) with *c-myc* and mutated *c-myc* DNA template; B) **InPy1** and **InPy2** (0–160 μM) with telomeric DNA template. Primer extension reaction at 50 °C. Conditions: 100 nM template, 50 nM primer, 0.2 mM dNTs, 5 mM KCl for *c-myc* template, 10 mM KCl for telomeric template, and 0.5 U *Taq* polymerase in enzyme buffer (50 mM Tris, 0.5 mM DTT, 0.1 mM EDTA, 5 mM $MgCl_2$, 5 mM KCl for *c-myc* template, and 10 mM KCl for telomeric template). P: primer, S: stop product, F: full-length product.

Molecular modeling and dynamics studies

To acquire insight into the binding mode and interactions of **InPy1** with *c-myc* and *c-kit* G-quadruplex DNA at the atomic level, molecular docking and dynamics studies were performed. Initially, energy-optimized **InPy1** (Figure S9, Supporting Information) at HF/6-31G* level in Gaussian 09[52] was docked with *c-myc* (PDB entry: 2L7V)[53] and *c-kit1* (PDB entry: 2O3M)[54] G-quadruplex DNAs using AutoDock 4.2.[55] The results reveal that **InPy1** stacks at both the top (top-**InPy1**) and bottom (bottom-**InPy1**) G-quartets of *c-myc* and *c-kit1* G-quadruplex DNAs (Figures S10 and S11, Supporting Information). This is in line with the experimentally observed 2:1 stoichiometry for the ligand–quadruplex complex. On the basis of docking results, 50 ns of unrestrained MD simulations were performed using AMBER 12.[56]

The binding free energy (ΔG) of the ligand and G-quadruplex was estimated by using the MM-PB/GBSA module in AMBER 12.[57] For the dual binding mode of **InPy1** with *c-myc* G-quadruplex DNA, the free energy was found to be -45.12 ± 7.43 kcal mol^{-1} (Table S1, Supporting Information). The preferred binding site of **InPy1** was the top quartet ($\Delta G = -22.56 \pm 4.13$ kcal mol^{-1}) over the bottom one ($\Delta G = -19.15 \pm 7.07$ kcal mol^{-1}; Table S1, Supporting Information). For the binding of **InPy1** with *c-kit1* G-quadruplex DNA, the free energy was found to be -43.78 ± 5.15 kcal mol^{-1} (Table S2, Supporting Information). Here, the preferred binding site was the bottom quartet ($\Delta G = -22.96 \pm 3.85$ kcal mol^{-1}) over the top ($\Delta G = -13.81 \pm 3.22$ kcal mol^{-1}). Similar to these results, a dual binding mode was also observed for derivatives of the natural product quindoline with *c-myc* G-quadruplex DNA.[53] To examine the structural stability of the G-quadruplex–ligand complex, the root mean square deviations (RMSDs) of the heavy atoms of the DNA backbone, G-quartet, and the top- and bottom-**InPy1** ligands were calculated with respect to the initial structure at each ps during 50 ns of MD simulations. The RMSD graphs (Figures S12 and S13, Supporting Information) and the average values (Table S3, Supporting Information) signify that G-quartet was stable during the MD simulation owing to the stacking interactions of two ligands at the bottom and top quartets of the G-quadruplex. Consequently, the percentage of Hoogsteen hydrogen bond occupancy (Table S4, Supporting Information) in the entire quartet was found to be >96% during MD simulation for both *c-myc* and *c-kit1* quadruplex structures.

The structure shown in the Figure 7 is the averaged MD snapshot of *c-myc* G-quadruplex DNA and **InPy1** from the last 15 ns of MD simulations. During the course of MD simulations,

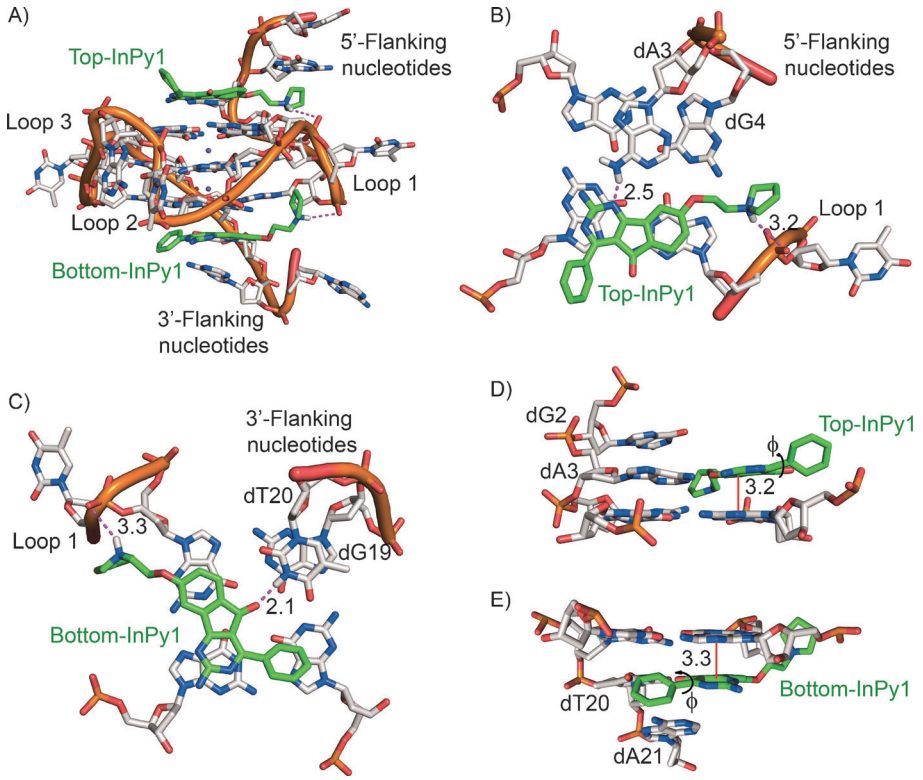

Figure 7. Averaged MD snapshot of **InPy1** with *c-myc* G-quadruplex DNA from the last 15 ns of 50 ns MD simulations. A) **InPy1** stacks at both the top and bottom G-quartet of *c-myc* G-quadruplex (2:1). B) **InPy1** and top quartet (axial view), showing hydrogen bonding and electrostatic interactions with the 5′-flanking nucleotide (dA3) and propeller loop, respectively. C) **InPy1** and bottom quartet (axial view), showing hydrogen bonding and electrostatic interactions with the 3′-flanking nucleotide (dT20) and propeller loop, respectively. D), E) Side view of top and bottom G-quartets with **InPy1**; the φ angle in the ligand and the stacking distance between **InPy1** and the G-quartet are indicated with red lines. Dashed magenta lines indicate the electrostatic interactions and hydrogen bond distances between the atoms in the ligands and G-quadruplex DNA; all distances are given in Å.

bottom-**InPy1** undergoes a significant re-orientation, which is evident by comparing the docked structure and the averaged MD structure (Figure 7C,E, and Figure S10, Supporting Information). This re-orientation occurs in order to avoid the steric clash between the benzene ring attached to the indenopyrimidine ring and 3′-flanking nucleotides. Moreover, the orientations of ligand at the top and the bottom quartet are quite different. At the bottom quartet, the keto group in the indenopyrimidine ring is oriented toward the 3′-flanking nucleotide. In contrast, at the top quartet, the amine group in the indenopyrimidine ring is directed toward the 5′-flanking nucleotide (Figure 7B,C).

For both top-**InPy1** and bottom-**InPy1**, the benzene ring attached to the pyrimidine ring is not in plane with respect to the indenopyrimidine ring of the ligand. The angle between the two rings (φ) was found to be in the range of 15–28° during the course of simulation. As a result, the benzene ring does not stack well on the G-quartet surface, and only the indenopyrimidine aromatic core stacks optimally on two guanine bases of the G-quartet (Figure 7D,E). The positively charged protonated pyrrolidine side chain makes electrostatic interactions with the negatively charged backbone in the propeller loop (loop-1) of *c-myc* G-quadruplex DNA (Figure 7B,C). Additionally, in the case of top-**InPy1**, the formation of a hydrogen bond between the nitrogen atom in the pyrimidine ring of the ligand and the NH_2 group of the 5′- flanking nucleotide (dA3) was observed at a distance of 2.5 ± 0.4 Å (Figure 7B). As illustrated in Figure 7C, the oxygen atom of the keto group in bottom-**InPy1** forms a hydrogen bond with the NH group of the 3′-flanking nucleotide (dT20) atom at a distance of 2.1 ± 0.5 Å. Above-mentioned electrostatic interactions and hydrogen bonds were observed for ~80% of the 50 ns simulation time.

The structure shown in the Figure 8A is the snapshot taken at the final step of MD simulation (50 ns) of *c-kit1* G-quadruplex DNA and **InPy1**. As apparent in Figure 8D, the two ligands are oriented perpendicular to each other. For both top- and bottom-**InPy1**, the amine group faces a flanking nucleotide (dT11 for top-**InPy1** and dA15 for bottom-**InPy1**), whereas the keto group faces the opposite side. Neither the top nor bottom ligand maintains the benzene ring in the plane of the indenopyrimidine ring. For bottom-**InPy1**, the φ value was found to be in the range between 36 and 51°. For top-**InPy1**, many fluctuations were observed, with the φ value varying from 20.8 to 54.1. It could be speculated that this out-of-plane orientation of the benzene ring pushes the entire ligand into a particular orientation (Figure 8D), with the benzene ring lying outside the quartets. Furthermore, in this orientation, very specific hydrogen bonds and other noncovalent interactions were observed between the quadruplex and **InPy1** (Figure 7 and Figure 8). The non-stacking nature of the benzene ring in **InPy1** with G-quadruplex DNA might contribute to the experimentally reported specificity of these ligands for promoter quadruplex DNA over telomeric DNA.

For bottom-**InPy1**, two hydrogen bonds were found to be present throughout the simulation (100% of the 50 ns run). The ether oxygen atom of the ligand and the amine of the flanking nucleotide (dG19) form a hydrogen bond at a distance of 2.38 ± 0.38 Å (Figure 8B). The hydrogen of the amine group in bottom-**InPy1** and the N3 atom of the flanking adenine (dA15) also make a hydrogen bond, with a distance of 2.04 ± 0.16 Å (Figure 8B). For top-**InPy1**, hydrogen bonds are visible only after ~10.75 ns of the MD run and are retained until the end of the simulation (78.5% of the simulation time). The two

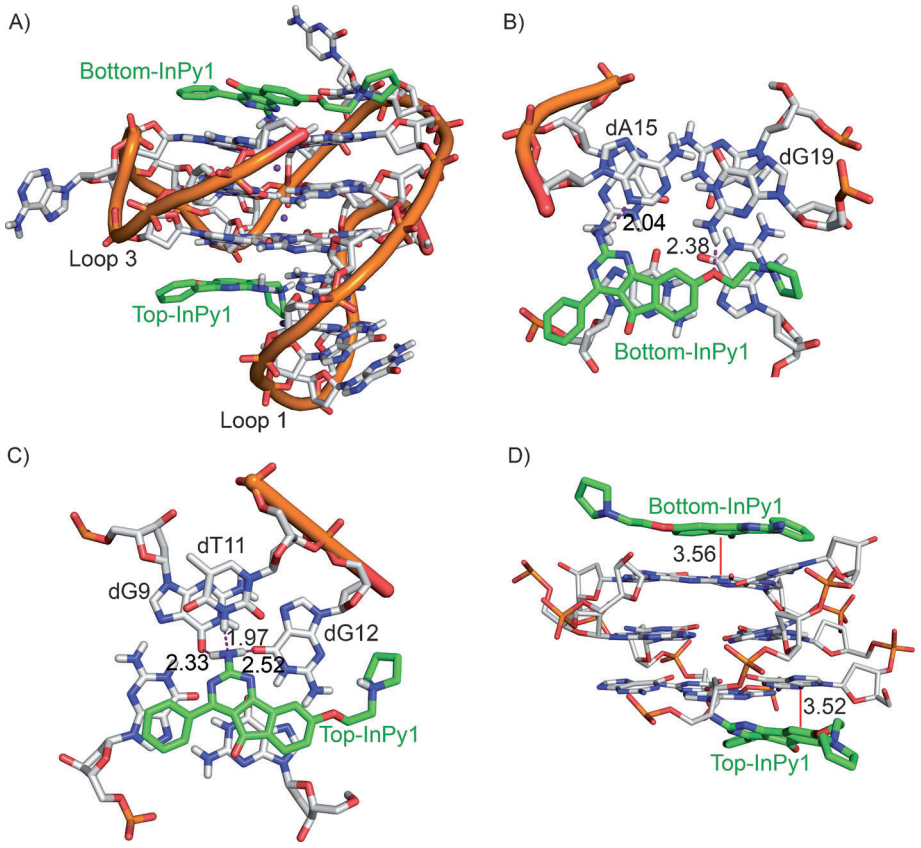

Figure 8. Final MD snapshot of **InPy1** with *c-kit1* G-quadruplex DNA after 50 ns MD simulation. A) **InPy1** and *c-kit1* G-quadruplex DNA (2:1): stacking occurs at both the top and bottom G-quartets of the G-quadruplex. B) **InPy1** and bottom quartet (axial view), showing the hydrogen bonding with flanking nucleotides (dG19 and dA15). C) **InPy1** and top quartet (axial view), showing the hydrogen bonding with the flanking nucleotide (dT11) and bottom quartet residues (dG9 and dG12). D) Side view of top and bottom **InPy1** with G-quartets, with red lines indicating the stacking distance between **InPy1** and G-quartets. Dashed magenta lines indicate the hydrogen bond distance between the atoms in ligand and G-quadruplex DNA; all distances are given in Å.

hydrogen atoms of the top-**InPy1** amine group form hydrogen bonds with the keto oxygen atom of the quartet guanines (dG12 and dG9), with average distances of 2.33 ± 0.52 and 2.52 ± 0.56 Å (Figure 8C). The nitrogen atom in the amine group of top-**InPy1** is hydrogen bonded with the hydrogen of NH in the flanking thymine (dT11), with an average distance of 1.97 ± 0.28 Å (Figure 8C). These studies demonstrate that the accurate positioning of the functional groups and side chains of **InPy1** can specifically identify the potential site in the loops and in the flanking nucleotides of promoter G-quadruplex DNAs to achieve optimal target recognition.

The unique ability of **InPy1** to make specific contacts with flanking nucleotides and the propeller loops present in parallel promoter G-quadruplex DNAs explains the specificity observed for this ligand. Overall, the MD simulations and binding free energy analysis rationalize the preferred 2:1 binding mode of **InPy1** with *c-myc* and *c-kit1* G-quadruplex structures.

Conclusions

Potential G-quadruplex-forming sequences present in the specific segments of the human genome such as telomeric ends and promoter regions of oncogenes have been known to form quadruplex structures of diverse topologies in in vitro and in vivo settings. Stabilizing such quadruplex structures with small molecules offers promise in the development of anticancer drugs. However, to develop a therapeutic agent armored with high precision, the molecules should be able to specifically bind and stabilize a particular quadruplex topology. In this direction, we have designed and synthesized a set of indenopyrimidine derivatives that contain an aromatic core containing side chains of varying length, terminated with amine functionalities. These molecules were screened for their binding interactions with quadruplex and duplex DNAs. CD titration experiments showed the property of ligands to induce a parallel topology for the *c-myc* and *c-kit* promoter quadruplex DNAs. CD melting studies validated the specific stabilization of promoter quadruplex DNAs over telomeric and duplex DNAs. The dual binding mode of the ligands with *c-myc* quadruplex DNA was confirmed by fluorescence titration as well as molecular modeling studies. In summary, these indenopyrimidine derivatives have emerged as specific G-quadruplex modulators and can be further engineered for potential therapeutic applications.

Experimental Section

Dry solvents (MeOH, DMF) were obtained from Merck and Spectrochem (India), and CH_3CN and CH_2Cl_2 were dried using CaH. Thin-layer chromatography (TLC) was performed on silica gel plates (Merck India) pre-coated with fluorescent indicator, with visualization by UV light (260 nm). Silica gel (100–200 mesh) was used for column chromatography. ^{13}C NMR (100 and 125 MHz) and ^{1}H NMR (400 and 500 MHz) data were recorded on 400 and 500 MHz instruments, respectively. Chemical shifts (δ, in parts per million) were referenced to the residual signal of deuterium solvents or TMS: TMS (0 ppm), CD_3OD (3.31 ppm), [D_6]DMSO (2.5 ppm) for ^{1}H NMR spectra; and $CDCl_3$ (77.2 ppm), CD_3OD (49.1 ppm), [D_6]DMSO (39.5 ppm) for ^{13}C NMR spectra. Multiplicities of ^{1}H NMR spin couplings are reported as s (singlet), d (doublet), t (triplet), q (quartet), dd (doublet of doublets), (q) quintet or m (multiplet and overlapping spin systems). Values for apparent coupling constants (J) are reported in Hz. High-resolution mass spectra (HRMS) were

obtained in positive-ion electrospray ionization (ESI) mode using a Q-TOF (micro, micromass) analyzer.

(*Z*)-2-Benzylidene-6-methoxy-2,3-dihydro-1*H*-inden-1-one (3).[38] 6-methoxyindanone **1** (1 g, 6.1 mmol) and benzaldehyde **2** (0.62 mL, 6.1 mmol) were dissolved in acetic acid (15 mL) with vigorous stirring. To this solution, 4–5 drops of concentrated HCl was added and held at reflux for 6 h. After completion, the reaction mixture was poured into 50 mL H_2O and was extracted with EtOAc (3×100 mL). The organic phase was dried over anhydrous Na_2SO_4, evaporated under reduced pressure, recrystallized from Et_2O and dried to give compound **3** as a light-yellow solid (1.29 g, 84%): R_f=0.8 (PE/EtOAc 8:2); ^{1}H NMR (400 MHz, [D$_6$]DMSO): δ=3.81 (s, 3H), 3.98 (s, 2H), 7.22 (d, J=2.5 Hz, 1H), 7.27 (dd, J=5.8, 2.5 Hz, 1H), 7.42–7.55 (m, 4H), 7.56 (d, J=8 Hz, 1H), 7.75 ppm (d, J=8 Hz, 2H); ^{13}C NMR (100 MHz, [D$_6$]DMSO): δ=31.2, 55.4, 105.5, 123.4, 127.5, 129.0, 129.8, 130.7, 132.7, 134.8, 135.8, 138.4, 142.6, 159.1, 193.1 ppm; HRMS: m/z $[M+H]^+$ calcd for $C_{17}H_{15}O_2$: 251.1072, found: 251.1079.

2-Amino-8-methoxy-4-phenyl-5*H*-indeno[1,2-*d*]pyrimidin-5-one (4).[38] Powdered NaOH (1.75 g, 43.8 mmol) was added to an EtOH solution (10 mL) of guanidine·HCl (4.18 g, 43.8 mmol) and was stirred for 0.5 h. The resulting solution was filtered to remove the precipitated NaCl, and the filtrate containing free guanine base was added to an EtOH suspension (8 mL) of compound **3** (730 mg, 2.92 mmol). The reaction mixture was held at reflux for 16 h, cooled for 30 min, filtered, and the precipitate was dried. The dried residue (450 mg) without purification was dissolved in DMF (10 mL), and powdered NaOH (140 mg, 3.5 mmol) was added. Air was bubbled through the reaction mixture using a needle, and was heated at 80 °C. After 16 h, the reaction mixture was cooled, and H_2O was added. The resulting precipitate was filtered, washed with H_2O and cold EtOH. The precipitate was dried to afford compound **4** as a dark-yellow solid (335 mg, 38%): R_f=0.4 (PE/EtOAc 7:3); ^{1}H NMR (400 MHz, [D$_6$]DMSO): δ=3.93 (s, 3H), 7.13 (dd, J=6.0, 2.2 Hz, 1H), 7.25 (d, J=2.2 Hz, 1H), 7.47–7.62 (m, 4H), 7.94 (br s, 2H), 8.00 ppm (d, J=6.7 Hz, 2H); ^{13}C NMR (100 MHz, [D$_6$]DMSO): δ=55.9, 106.2, 111.5, 117.8, 125.0, 127.6, 130.7, 128.8, 129.5, 130.7, 135.7, 142.2, 164.2, 164.2, 164.9, 174.8, 186.6 ppm; HRMS: m/z $[M+H]^+$ calcd for $C_{18}H_{14}N_3O_2$: 304.1086, found: 304.1078.

2-Amino-8-hydroxy-4-phenyl-5*H*-indeno[1,2-*d*]pyrimidin-5-one (5).[38] Compound **4** (90 mg, 0.3 mmol) was dissolved in *N*-methyl-2-pyrrolidone together with LiCl (254 mg, 6 mmol) and H_2O (0.2 mL). The reaction mixture was heated at 180 °C for 2–3 days and was diluted with THF and EtOAc, washed with H_2O and brine. The organic phase was dried over anhydrous Na_2SO_4, evaporated under reduced pressure and dried to give compound **5** as a yellow solid (80 mg, 94%): R_f=0.5 (PE/EtOAc 6:4); ^{1}H NMR (400 MHz, [D$_6$]DMSO): δ=6.94 (dd, J=6.0, 2.5 Hz, 1H), 7.15 (d, J=2.0 Hz, 1H), 7.46–7.54 (m, 4H), 7.88 (br s, 2H), 7.99 (d, J=6.5 Hz, 2H), 10.79 ppm (br s, 1H); ^{13}C NMR (100 MHz, [D$_6$]DMSO): δ=107.9, 111.7, 118.9, 125.4, 127.5, 127.7, 129.6, 130.7, 135.8, 142.4, 163.3, 164.0, 164.9, 175.1, 186.8 ppm; HRMS: m/z $[M+H]^+$ calcd for $C_{17}H_{12}N_3O_2$: 290.0930, found: 290.0938.

2-Amino-8-(2-bromoethoxy)-4-phenyl-5*H*-indeno[1,2-*d*]pyrimidin-5-one (6). Compound **5** (85 mg, 0.3 mmol) was dissolved in dry CH_3CN (3 mL), anhydrous K_2CO_3 (124 mg, 0.9 mmol) and 1,2-dibromoethane (0.11 mL, 1.2 mmol) were added, and the mixture was heated at 75 °C for 18 h. The solvent was evaporated, and the crude compound was purified by column chromatography (20% EtOAc in hexane) to give **6** as a yellow solid (94 mg, 80%): R_f=0.5 (PE/EtOAc 7:3); ^{1}H NMR (500 MHz, [D$_6$]DMSO): δ=3.86 (t, J=5.1 Hz, 2H), 4.51 (t, J=5.0 Hz, 2H), 7.17 (dd, J=8.2, 2.1 Hz, 1H), 7.26 (d, J=2.1 Hz, 1H), 7.46–7.57 (m, 3H), 7.61 (d, J=8.2 Hz, 1H), 7.90 (br s, 2H), 8.00 ppm (d, J=7.0 Hz, 2H); ^{13}C NMR (125 MHz, [D$_6$]DMSO): δ=31.6, 68.9, 107.1, 112.0, 119.1, 125.5, 128.1, 129.7, 130.0, 131.2, 136.1, 142.7, 163.3, 164.7, 165.4, 175.3, 187.0 ppm; HRMS: m/z $[M+H]^+$ calcd for $C_{19}H_{15}N_3O_2Br$: 396.0348, found: 396.0350.

2-Amino-8-(3-bromopropoxy)-4-phenyl-5*H*-indeno[1,2-*d*]pyrimidin-5-one (7). To a solution of **5** (85 mg, 0.3 mmol) in dry CH_3CN (3 mL), anhydrous K_2CO_3 (124 mg, 1.2 mmol) and 1,2-dibromopropane (0.12 mL, 1.2 mmol) were added, and the reaction mixture was heated at 75 °C for 18 h. The solvent was evaporated, and the crude mixture was purified by column chromatography (20% EtOAc in hexane) to give compound **7** as yellow solid (102 mg, 83%): R_f=0.7 (PE/EtOAc 7:3); ^{1}H NMR (400 MHz, [D$_6$]DMSO): δ=2.29 (q, J=6.0 Hz, 2H), 3.69 (t, J=6.6 Hz, 2H), 4.23 (t, J=6.0 Hz, 2H), 7.13 (dd, J=6.0, 2.2 Hz, 1H), 7.24 (d, J=2.2 Hz, 1H), 7.46–7.59 (m, 4H), 7.92 (br s, 2H), 7.99 ppm (d, J=6.6 Hz, 2H); ^{13}C NMR (100 MHz, [D$_6$]DMSO): δ=31.0, 31.6, 66.3, 106.5, 111.5, 118.3, 125.0, 127.6, 128.9, 129.5, 130.7, 135.6, 142.2, 163.3, 164.2, 164.9, 174.8, 186.6 ppm; HRMS: m/z $[M+H]^+$ calcd for $C_{20}H_{17}N_3O_2Br$: 410.0504, found: 410.0484.

2-Amino-4-phenyl-8-(2-(pyrrolidin-1-yl)ethoxy)-5*H*-indeno[1,2-*d*]-pyrimidin-5-one (InPy1). To a solution of **6** (50 mg, 0.09 mmol) in dry CH_3CN (2 mL), pyrrolidine (0.02 mL, 0.28 mmol) was added, and the resulting reaction mixture was held at reflux for 12 h. The solvent was evaporated, and the crude product was purified by column chromatography using basic alumina as a stationary phase (3% MeOH in CH_2Cl_2) to afford compound **InPy1** as a yellow solid (30 mg, 86%): R_f=0.3 (CH_2Cl_2/MeOH 9.6:0.4); ^{1}H NMR (400 MHz, $CDCl_3$): δ=1.83 (br s, 4H), 2.67 (br s, 4H), 2.97 (t, J=5.7 Hz, 2H), 4.25 (t, J=5.7 Hz, 2H), 5.81 (br s, 2H), 7.02 (dd, J=8.2, 2.2 Hz, 1H), 7.35 (d, J=2.2 Hz, 1H), 7.45–7.54 (m, 3H), 7.65 (d, J=8.2 Hz, 1H), 8.05 ppm (dd, J=7.6, 1.8 Hz, 2H); ^{13}C NMR (100 MHz, $CDCl_3$): δ=23.6, 54.9, 54.9, 67.9, 107.1, 114.0, 118.8, 125.5, 128.1, 129.4, 129.8, 131.2, 135.6, 142.6, 164.1, 164.7, 164.2, 176.0, 187.7 ppm; HRMS: m/z $[M+H]^+$ calcd for $C_{23}H_{23}N_4O_2$: 387.1821, found: 387.1813.

2-Amino-8-(3-cyclopentylpropoxy)-4-phenyl-5*H*-indeno[1,2-*d*]-pyrimidin-5-one (InPy2). To a solution of compound **7** (50 mg, 0.12 mmol) in dry CH_3CN (2 mL), pyrrolidine (0.03 mL, 0.37 mmol) was added, and the reaction mixture was held at reflux for 12 h. The solvent was evaporated, and the crude product was purified by column chromatography using basic alumina as a stationary phase (3% MeOH in CH_2Cl_2) to afford compound **InPy2** as a yellow solid (40 mg, 95%): R_f=0.3 (CH_2Cl_2/MeOH 9.6:0.4); ^{1}H NMR (400 MHz, CD_3OD): δ=1.87 (br s, 4H), 2.06 (q, J=6.4 Hz, 2H), 2.69 (br s, 4H), 2.75 (t, J=6.9 Hz, 2H), 4.14 (t, J=5.9 Hz, 2H), 7.03 (d, J=8.0 Hz, 1H), 7.33 (br s, 1H), 7.43–7.60 (m, 4H), 8.02 ppm (d, J=7.0 Hz, 2H); ^{13}C NMR (100 MHz, CD_3OD): δ=24.2, 30.8, 55.2, 67.4, 68.8, 108.4, 109.7, 113.6, 119.1, 120.2, 126.2, 128.9, 131.0, 132.0, 137.2, 143.7, 165.4, 166.5, 176.9, 189.0 ppm; HRMS: m/z $[M+H]^+$ calcd for $C_{24}H_{25}N_4O_2$: 401.1978, found: 401.1968.

2-Amino-8-(2-(2-(dimethylamino)ethylamino)ethoxy)-4-phenyl-5*H*-indeno[1,2-*d*]pyrimidin-5-one (InPy3). To a solution of compound **6** (40 mg, 0.09 mmol) in dry CH_3CN (2 mL), *N*,*N*-dimethylethane-1,2-diamine (0.03 mL, 0.29 mmol) was added, and the reaction mixture was held at reflux for 12 h. The solvent was evaporated, and the crude product was purified by column chromatography using basic alumina as a stationary phase (5% MeOH in CH_2Cl_2) to afford **InPy3** as a dark-yellow solid (30 mg, 83%): R_f=0.4 (CH_2Cl_2/MeOH 9.5:0.5); ^{1}H NMR (400 MHz, $CDCl_3$): δ=1.99 (s, 1H),

2.25 (s, 6H), 2.53 (t, J=6.0 Hz, 2H), 2.82 (t, J=6.0 Hz, 2H), 3.07 (t, J=4.7 Hz, 2H), 4.19 (t, J=4.7 Hz, 2H), 6.15 (brs, 2H), 6.98 (d, J=8.0 Hz, 1H), 7.30 (brs, 1H), 7.44–7.54 (m, 3H), 7.61 (d, J=8.2 Hz, 1H), 8.03 ppm (dd, J=7.4, 1.9 Hz, 2H); ^{13}C NMR (125 MHz, $CDCl_3$): δ=45.1, 46.6, 48.4, 58.4, 67.9, 107.0, 113.6, 118.5, 125.4, 128.0, 129.3, 129.7, 131.1, 135.4, 142.4, 163.9, 164.5, 165.0, 175.7, 187.5 ppm; HRMS: m/z $[M+H]^+$ calcd for $C_{23}H_{26}N_5O_2$: 404.2087, found: 404.2080.

Ligand stock solution preparation. Stock solutions for all ligands were made to 10 mM in DMSO. They were further diluted to 1 mM by using 10 mM HCl for all experiments.

Oligonucleotides. All oligonucleotides were synthesized at 1 μM scales using appropriate controlled pore glass (CPG) as a 3′-solid support in a Mermade-4 DNA/RNA synthesizer and were purified by 20% PAGE. The concentration of all oligonucleotides was measured at 260 nm in a UV/Vis spectrophotometer using appropriate molar extinction coefficients. The following oligonucleotides were used for CD titration, melting, and fluorescence experiments: telomeric DNA (5′-AGG GTT AGG GTT AGG GTT AGG G-3′), wild-type *c-myc* DNA (5′-TGA GGG TGG GGA GGG TGG GGA A-3′), *c-kit1* DNA (5′-GGG AGG GCG CTG GGA GGA GGG-3′), and duplex DNA (5′-CCA GTT CGT AGT AAC CC-3′ and the complementary sequence 5′-GGG TTA CTA CGA ACT GG-3′). For *Taq* DNA polymerase stop assays, the primer sequence (5′-ACG ACT CAC TAT AGC AAT TGC G-3′), template containing wild-type *c-myc* sequence (5′-TGA GGG TGG GGA GGG TGG GGA AGC CAC CGC AAT TGC TAT AGT GAG TCG T-3′), mutated *c-myc* sequence (5′-TGA GGG TGG GTA GAG TGG GTA AGC CAC CGC AAT TGC TAT AGT GAG TCG T-3′), and template containing human telomeric sequence (5′-AGG GTT AGG GTT AGG GTT AGG GGC CAC CGC AAT TGC TAT AGT GAG TCG T-3′) were used.

CD titration studies. CD spectra were recorded on a Jasco 815 CD spectrophotometer in the wavelength range of 220–320 nm using a quartz cuvette with 1.0 mm path length. The scanning speed of the instrument was set at 100 nm min^{-1}, and the response time was 2 s. Baseline was measured using 50 mM Tris buffer (pH 7.2) for experiments without salts, and with 100 mM KCl for the experiments in the presence of salts. The strand concentration of oligonucleotide used was 12.5 μM. Each spectrum is an average of three measurements at 25 °C. All spectra were analyzed using Origin 8.0 software.

CD melting studies. For melting studies, 10–15 μM strand concentration of oligonucleotide in 10 mM lithium cacodylate (pH 7.2), the required amount of monovalent salts (LiCl and KCl) and 5 mol equiv ligands (50–75 μM) were used. Telomeric DNA (10 μM DNA in 10 mM KCl for K^+ conditions, and 10 mM NaCl, 10 mM sodium cacodylate for Na^+ conditions (pH 7.2) and 90 mM LiCl), *c-kit1* DNA (10 μM DNA in 10 mM KCl and 90 mM LiCl), *c-myc* DNA (10 μM in 1 mM KCl and 99 mM LiCl) and duplex DNA (15 μM in 10 mM KCl and 90 mM LiCl) were annealed by heating at 95 °C for 5 min, followed by gradual cooling to room temperature. Ligands (5 equiv) were added to the annealed DNAs and were kept at 4 °C overnight. Thermal melting was monitored at 295, 263, and 242 nm for telomeric, promoter, and duplex DNAs, respectively, at a heating rate of 1 °C min^{-1}. The melting temperatures were determined from sigmoidal curve fit using the Boltzmann function in Origin 8.0 software.

Fluorescence titration experiments. Fluorimetric titrations were performed on a Cary Eclipse spectrofluorimeter by using a 1 mL quartz cuvette with a 1 cm path length. Emission spectra for **InPy1** (100 μM) were recorded in the wavelength range of 360–700 nm with an excitation wavelength of 350 nm, and for **InPy2** in the wavelength range of 362–700 nm after an excitation at 352 nm. DNA was pre-annealed in the presence of 100 mM KCl and 10 mM lithium cacodylate buffer by heating at 95 °C and gradual cooling to room temperature over 4–5 h. The ligand concentration used was 100 μM and was titrated with increasing concentrations of DNA (0–30 μM). Fluorescence intensity (F/F_o) was plotted against DNA concentration, and binding constants were calculated by curve fitting using the Stern–Volmer equation, $F/F_o = 1 + K_a$[DNA], in which F and F_o are the fluorescence intensities of the ligand in the presence and absence of DNA, respectively, [DNA] is the concentration of DNA, and K_a is the binding constant. Job plot analysis for **InPy1** with *c-myc* was performed with an excitation wavelength of 350 nm and emission spectra were recorded in the range of 360–700 nm. The total concentration of ligand + DNA complex was kept constant at 5 μM. Samples were prepared by varying the mole fractions (0–1) of **InPy1** in the sample. Mole fractions of **InPy1** were plotted against the fluorescence intensities to obtain the stoichiometry for ligand–DNA complexes. All curves were analyzed by Origin 8.0 software.

5′-End radiolabeling of oligonucleotides. DNA (10 pmol) was 5′-end labeled by T4 polynucleotide kinase (PNK; 5 U) in 1×PNK buffer for forward reaction [50 mM Tris·HCl pH 7.6, 10 mM $MgCl_2$, 5 mM DTT, 0.1 mM each spermidine and 0.1 mM EDTA] and [γ-^{32}P]ATP (370 Ci mmol^{-1} in 3 μL) in a total volume of 10 μL for 1 h at 37 °C followed by deactivation of the enzyme by heating at 70 °C for 3 min. The end-labeled DNA was then purified using a QIAquick Nucleotide removal kit protocol provided by the manufacturer (Qiagen).

***Taq* DNA polymerase stop assays**. These assays were performed using reported procedures.[51] Appropriate amounts of labeled primer oligonucleotide (~20000 cpm) were mixed with cold primer (50 nM) and template (100 nM), and they were annealed in an annealing buffer [5 mM Tris (pH 8), 15 mM NaCl, 0.1 mM EDTA] by heating at 95 °C for 5 min and then gradual cooling to room temperature over 4–5 h. The annealed primer–template was mixed with 1× polymerase buffer [50 mM Tris, 0.5 mM DTT, 0.1 mM EDTA, 5 mM $MgCl_2$, 5 mM KCl for *c-myc* template and 10 mM KCl for telomeric template], 1 μg μL^{-1} BSA, and 0.2 mM dNTPs. The ligands in appropriate concentrations were added to the reaction mixture (10 μL total volume) and incubated for 30 min at room temperature. Finally, the primer-extension reaction was initiated by adding *Taq* DNA polymerase (0.5 U) and incubated at 50 °C for *c-myc* and at 40 °C for telomeric DNA for 30 min. The extension reaction was stopped by adding 10 μL 2× stop buffer (10 mM EDTA, 10 mM NaOH, 0.1% each bromophenol blue (*w/v*) and xylene cyanol (*w/v*) in formamide). Samples were analyzed in 15% denaturing PAGE in which 1× TBE (89 mM each of Tris and boric acid and 2 mM EDTA, pH ~8.3) was used as running buffer, and gels were imaged by autoradiography with a PhosphorImager; quantification of gels was performed using ImageQuant 5.2 software.

Molecular modeling. The coordinates of *c-myc* (PDB entry: 2L7V) and *c-kit1* (PDB entry: 2O3M) G-quadruplex DNA structures were retrieved and prepared for docking; the **InPy1** structure was optimized using Gaussian 09[52] (HF/6-31G* level). Using AutoDock 4.2,[55] docking studies were carried out with the Lamarckian genetic algorithm following the procedure developed for G-quadruplex DNA and ligand docking. To facilitate the docking to *c-kit1* DNA, terminal 5′-nucleotide dA1 was removed from the PDB file. Subsequent to the docking studies, MD simulations were carried out using AMBER 12.[56] The procedure for MD simulations was used from the protocol developed by Haider and Neidle.[58] Briefly, RESP[59] charge fitted **InPy1** was complexed with *c-myc* and *c-kit1*

G-quadruplex DNA (2:1) using Generalized AMBER force field (GAFF)[60] and AMBER FF10SB, respectively. The system was then solvated using TIP3P water molecules extended up to 12 Å in an octahedral box. The neutrality of the system was achieved by adding K^+ ions. The solvated system was then subjected to equilibration followed by 50 ns of MD simulation with coordinates saved for each ps. Binding free energy of ligands were estimated using MM-PB/GBSA methods,[57] RMSDs of the heavy atoms, Hoogsteen hydrogen bonding occupancies, and dihedral angles were calculated using the ptraj module. Figures were rendered using PyMOL (http://www.pymol.org).

Acknowledgements

We are thankful to the Computer Centre, IIT Bombay, for use of the HPC facility; to Prof. David A. Case (Rutgers University) for waiving the licensing fee for AMBER 12; and to Prof. Ruchi Anand (IIT Bombay) for providing access to her laboratory facilities. This work is supported financially by a grant from the Department of Atomic Energy—Board of Research in Nuclear Sciences (DAE-BRNS; grant no: 2012/37C/4/BRNS-1063). K.V.D. and S.H. thank the Council of Scientific and Industrial Research (CSIR) and DAE-BRNS, respectively, for their fellowships.

Keywords: DNA · G-quadruplexes · indenopyrimidines · promoters · specificity

[1] S. Burge, G. N. Parkinson, P. Hazel, A. K. Todd, S. Neidle, *Nucleic Acids Res.* **2006**, *34*, 5402 – 5415.
[2] P. Murat, Y. Singh, E. Defrancq, *Chem. Soc. Rev.* **2011**, *40*, 5293 – 5307.
[3] S. Balasubramanian, S. Neidle, *Curr. Opin. Chem. Biol.* **2009**, *13*, 345 – 353.
[4] J. L. Huppert, S. Balasubramanian, *Nucleic Acids Res.* **2007**, *35*, 406 – 413.
[5] S. Balasubramanian, L. H. Hurley, S. Neidle, *Nat. Rev. Drug Discovery* **2011**, *10*, 261 – 275.
[6] Y. Qin, L. H. Hurley, *Biochimie* **2008**, *90*, 1149 – 1171.
[7] V. González, L. H. Hurley, *Annu. Rev. Pharmacol. Toxicol.* **2010**, *50*, 111 – 129.
[8] J. Seenisamy, E. M. Rezler, T. J. Powell, D. Tye, V. Gokhale, C. S. Joshi, A. Siddiqui-Jain, L. H. Hurley, *J. Am. Chem. Soc.* **2004**, *126*, 8702 – 8709.
[9] T. Simonsson, P. Pecinka, M. Kubista, *Nucleic Acids Res.* **1998**, *26*, 1167 – 1172.
[10] S. Rankin, A. P. Reszka, J. Huppert, M. Zloh, G. N. Parkinson, A. K. Todd, S. Ladame, S. Balasubramanian, S. Neidle, *J. Am. Chem. Soc.* **2005**, *127*, 10584 – 10589.
[11] D. Sen, W. Gilbert, *Nature* **1990**, *344*, 410 – 414.
[12] a) A. Risitano, K. R. Fox, *Nucleic Acids Res.* **2004**, *32*, 2598 – 2606; b) P. Hazel, J. Huppert, S. Balasubramanian, S. Neidle, *J. Am. Chem. Soc.* **2004**, *126*, 16405 – 16415; c) M. Cevec, J. Plavec, *Biochemistry* **2005**, *44*, 15238 – 15246; d) P. A. Rachwal, I. S. Findlow, J. M. Werner, T. Brown, K. R. Fox, *Nucleic Acids Res.* **2007**, *35*, 4214 – 4222; e) P. A. Rachwal, T. Brown, K. R. Fox, *FEBS Lett.* **2007**, *581*, 1657 – 1660.
[13] T. Qu, Y. Lu, J. Jan, Z. Huang, K. Wong, L. Gu, *ChemMedChem* **2008**, *3*, 690 – 713.
[14] D. Monchaud, M. P. Teulade-Fichou, *Org. Biomol. Chem.* **2008**, ***6***, 627 – 636.
[15] Q. Li, J. F. Xiang, H. Zhang, Y. L. Tang, *Curr. Pharm. Des.* **2012**, *18*, 1973 – 1983.
[16] D. L. Ma, T. S. Lai, F. Y. Chan, W. H. Chung, R. Abagyan, Y. C. Leung, K. Y. Wong, *ChemMedChem* **2008**, *3*, 881 – 884.
[17] S. Cosconati, A. Rizzo, R. Trotta, B. Pagano, S. Iachettini, S. D. Tito, I. Lauri, I. Fotticchia, M. Giustiniano, L. Marinelli, C. Giancola, E. Novellino, A. Biroccio, A. Randazzo, *J. Med. Chem.* **2012**, *55*, 9785 – 9792.
[18] S. A. Ohnmacht, S. Neidle, *Bioorg. Med. Chem. Lett.* **2014**, *24*, 2602 – 2612.
[19] R. T. Wheelhouse, D. Sun, H. Han, F. X. Han, L. H. Hurley, *J. Am. Chem. Soc.* **1998**, *120*, 3261 – 3262.
[20] C. Romera, O. Bombarde, R. Bonnet, D. Gomez, P. Dumy, P. Calsou, J. F. Gwan, J. H. Lin, E. Defrancq, G. Pratviel, *Biochimie* **2011**, *93*, 1310 – 1317.
[21] P. Wang, L. Ren, H. He, F. Liang, X. Zhou, Z. Tan, *ChemBioChem* **2006**, *7*, 1155 – 1159.
[22] M. Y. Kim, H. Vankayalapati, K. Shin-Ya, K. Wierzba, L. H. Hurley, *J. Am. Chem. Soc.* **2002**, *124*, 2098 – 2099.
[23] M. Read, R. J. Harrison, B. Romagnoli, F. A. Tanious, S. H. Gowan, A. P. Reszka, W. D. Wilson, L. R. Kelland, S. Neidle, *Proc. Natl. Acad. Sci. USA* **2001**, *98*, 4844 – 4849.
[24] C. Sissi, L. Lucatello, A. P. Krapcho, D. J. Maloney, M. B. Boxer, M. V. Camarasa, G. Pezzoni, E. Menta, M. Palumbo, *Bioorg. Med. Chem.* **2007**, *15*, 555 – 562.
[25] W. Duan, A. Rangan, H. Vankayalapati, M. Y. Kim, Q. Zeng, D. Sun, H. Han, O. Y. Fedoroff, D. Nishioka, S. Young Rha, E. Izbicka, D. D. Von Hoff, L. H. Hurley, *Mol. Cancer Ther.* **2001**, *1*, 103 – 120.
[26] M. Franceschin, A. Alvino, V. Casagrande, C. Mauriello, E. Pascucci, M. Savino, G. Ortaggi, A. Bianco, *Bioorg. Med. Chem.* **2007**, *15*, 1848 – 1858.
[27] S. Sparapani, S. M. Haider, F. Doria, M. Gunaratnam, S. Neidle, *J. Am. Chem. Soc.* **2010**, *132*, 12263 – 12272.
[28] F. Hamon, E. Largy, A. Gudin-Beaurepaire, M. Rouchon-Dagois, A. Sidibe, D. Monchaud, J. L. Mergny, J. F. Riou, C. H. Nguyen, M. P. Teulade-Fichou, *Angew. Chem. Int. Ed.* **2011**, *50*, 8745 – 8749; *Angew. Chem.* **2011**, *123*, 8904 – 8908.
[29] J. M. Nicoludis, S. T. Miller, P. D. Jeffrey, S. P. Barrett, P. R. Rablen, T. J. Lawton, L. A. Yatsunyk, *J. Am. Chem. Soc.* **2012**, *134*, 20446 – 20456.
[30] N. C. Sabharwal, V. Savikhin, J. R. Turek-Herman, J. M. Nicoludis, V. A. Szalai, L. A. Yatsunyk, *FEBS J.* **2014**, *281*, 1726 – 1737.
[31] R. V. Brown, F. L. Danford, V. Gokhale, L. H. Hurley, T. A. Brooks, *J. Biol. Chem.* **2011**, *286*, 41018 – 41027.
[32] P. V. L. Boddupally, S. Hahn, C. Beman, B. De, T. A. Brooks, V. Gokhale, L. H. Hurley, *J. Med. Chem.* **2012**, *55*, 6076 – 6086.
[33] J. Dash, R. N. Das, N. Hegde, G. D. Pantos, P. S. Shirude, S. Balasubramanian, *Chem. Eur. J.* **2012**, *18*, 554 – 564.
[34] J. Dash, P. S. Shirude, S.-T. D. Hsu, S. Balasubramanian, *J. Am. Chem. Soc.* **2008**, *130*, 15950 – 15956.
[35] T. Agarwal, S. Roy, T. K. Chakraborty, S. Maiti, *Biochemistry* **2010**, *49*, 8388 – 8397.
[36] V. Dhamodharan, S. Harikrishna, C. Jagadeeswaran, K. Halder, P. I. Pradeepkumar, *J. Org. Chem.* **2012**, *77*, 229 – 242.
[37] K. Gracie, V. Dhamodharan, P. I. Pradeepkumar, K. Faulds, D. Graham, *Analyst* **2014**, *139*, 4458 – 4465.
[38] B. C. Shook, S. Rassnick, N. Wallace, J. Crooke, M. Ault, D. Chakravarty, J. K. Barbay, A. Wang, M. T. Powell, K. Leonard, V. Alford, R. H. Scannevin, K. Carroll, L. Lampron, L. Westover, H. K. Lim, R. Russell, S. Branum, K. M. Wells, S. Damon, S. Youells, X. Li, D. A. Beauchamp, K. Rhodes, P. F. Jackson, *J. Med. Chem.* **2012**, *55*, 1402 – 1417.
[39] F. C. Meng, F. Mao, W. J. Shan, F. Qin, L. Huang, X. S. Li, *Bioorg. Med. Chem. Lett.* **2012**, *22*, 4462 – 4466.
[40] S. Paramasivan, I. Rujan, H. P. Bolton, *Methods* **2007**, *43*, 324 – 331.
[41] A. Ambrus, D. Chen, J. Dai, T. Bialis, R. A. Jones, D. Yang, *Nucleic Acids Res.* **2006**, *34*, 2723 – 2735.
[42] E. M. Rezler, J. Seenisamy, S. Bashyam, K. Mu-Yong, E. White, W. D. Wilson, L. H. Hurley, *J. Am. Chem. Soc.* **2005**, *127*, 9439 – 9447.
[43] A. Guédin, L. Lacroix, J. L. Mergny, *Methods Mol. Biol.* **2010**, *613*, 25 – 35.
[44] J. Mohanty, N. Barooh, V. Dhamodharan, S. Harikrishna, P. I. Pradeepkumar, A. C. Bhasikuttan, *J. Am. Chem. Soc.* **2013**, *135*, 367 – 376.
[45] Y. P. Kumar, S. Bhowmik, R. N. Das, I. Bessi, S. Paladhi, R. Ghosh, H. Schwalbe, J. Dash, *Chem. Eur. J.* **2013**, *19*, 11502 – 11506.
[46] S. Shi, J. Zhao, X. Geng, T. Yao, H. Huang, T. Liu, L. Zheng, Z. Li, D. Yang, L. Ji, *Dalton Trans.* **2010**, *39*, 2490 – 2493.
[47] A. Arora, C. Balasubramanian, N. Kumar, S. Agrawal, R. P. Ojha, S. Maiti, *FEBS J.* **2008**, *275*, 3971 – 3983.
[48] N. Ranjan, D. P. Arya, *Molecules* **2013**, *18*, 14228 – 14240.
[49] C. Wei, Y. Wang, M. Zhang, *Org. Biomol. Chem.* **2013**, *11*, 2355 – 2364.
[50] A. Cummaro, I. Fotticchia, M. Franceschin, C. Giancola, L. Petraccone, *Biochimie* **2011**, *93*, 1392 – 1400.

[51] a) H. Han, L. H. Hurley, M. Salazar, *Nucleic Acids Res.* **1999**, *27*, 537 – 542; b) J. Seenisamy, S. Bashyam, V. Gokhale, H. Vankayalpati, C. L. Grand, A. Siddiqui-Jain, N. Streiner, W. D. Wilson, L. H. Hurley, *J. Am. Chem. Soc.* **2005**, *127*, 2944 – 2959.

[52] M. J. Frisch, G. W. Trucks, H. B. Schlegel, G. E. Scuseria, M. A. Robb, J. R. Cheeseman, G. Scalmani, V. Barone, B. Mennucci, G. A. Petersson, H. Nakatsuji, M. Caricato, X. Li, H. P. Hratchian, A. F. Izmaylov, J. Bloino, G. Zheng, J. L. Sonnenberg, M. Hada, M. Ehara, K. Toyota, R. Fukuda, J. Hasegawa, M. Ishida, T. Nakajima, Y. Honda, O. Kitao, H. Nakai, T. Vreven, J. A. Montgomery, Jr., J. E. Peralta, F. Ogliaro, M. Bearpark, J. J. Heyd, E. Brothers, K. N. Kudin, V. N. Staroverov, R. Kobayashi, J. Normand, K. Raghavachari, A. Rendell, J. C. Burant, S. S. Iyengar, J. Tomasi, M. Cossi, N. Rega, J. M. Millam, M. Klene, J. E. Knox, J. B. Cross, V. Bakken, C. Adamo, J. Jaramillo, R. Gomperts, R. E. Stratmann, O. Yazyev, A. J. Austin, R. Cammi, C. Pomelli, J. W. Ochterski, R. L. Martin, K. Morokuma, V. G. Zakrzewski, G. A. Voth, P. Salvador, J. J. Dannenberg, S. Dapprich, A. D. Daniels, Ö. Farkas, J. B. Foresman, J. V. Ortiz, J. Cioslowski, D. J. Fox, *Gaussian 09*, *Revision A.02*, Gaussian Inc., Wallingford, CT (USA), **2009**.

[53] J. Dai, M. Carver, L. H. Hurley, D. Yang, *J. Am. Chem. Soc.* **2011**, *133*, 17673 – 17680.

[54] A. T. Phan, V. V. Kuryavyi, S. Burge, S. Neidle, D. J. Patel, *J. Am. Chem. Soc.* **2007**, *129*, 4386 – 4392.

[55] G. M. Morris, D. S. Goodsell, R. S. Halliday, R. Huey, W. E. Hart, R. K. Belew, A. J. Olson, *J. Comput. Chem.* **1998**, *19*, 1639 – 1662.

[56] D. A. Case, *AMBER 12*, University of California, San Francisco, CA (USA), **2012**.

[57] P. A. Kollman, I. Massova, C. Reyes, B. Kuhn, S. Huo, L. Chong, M. Lee, T. Lee, Y. Duan, W. Wang, O. Donini, P. Cieplak, J. Srinivasan, D. A. Case, T. E. Cheatham, *Acc. Chem. Res.* **2000**, *33*, 889 – 897.

[58] S. Haider, S. Neidle, *Methods Mol. Biol.* **2010**, *608*, 17 – 37.

[59] T. Fox, P. A. Kollman, *J. Phys. Chem. B* **1998**, *102*, 8070 – 8079.

[60] J. Wang, R. M. Wolf, J. W. Caldwell, P. A. Kollman, D. A. Case, *J. Comput. Chem.* **2004**, *25*, 1157 – 1174.

Received: September 13, 2014
Published online on October 30, 2014

CHEMMEDCHEM
Chemistry & Drug Discovery

Supporting Information

Targeting Promoter G-Quadruplex DNAs by Indenopyrimidine-Based Ligands

K. V. Diveshkumar, Saaz Sakrikar, S. Harikrishna, V. Dhamodharan, and P. I. Pradeepkumar*[a]

cmdc_201402394_sm_miscellaneous_information.pdf

TABLE OF CONTENTS

CD spectra for ligands with telomeric DNA in the absence/presence of K^+/Na^+ ions

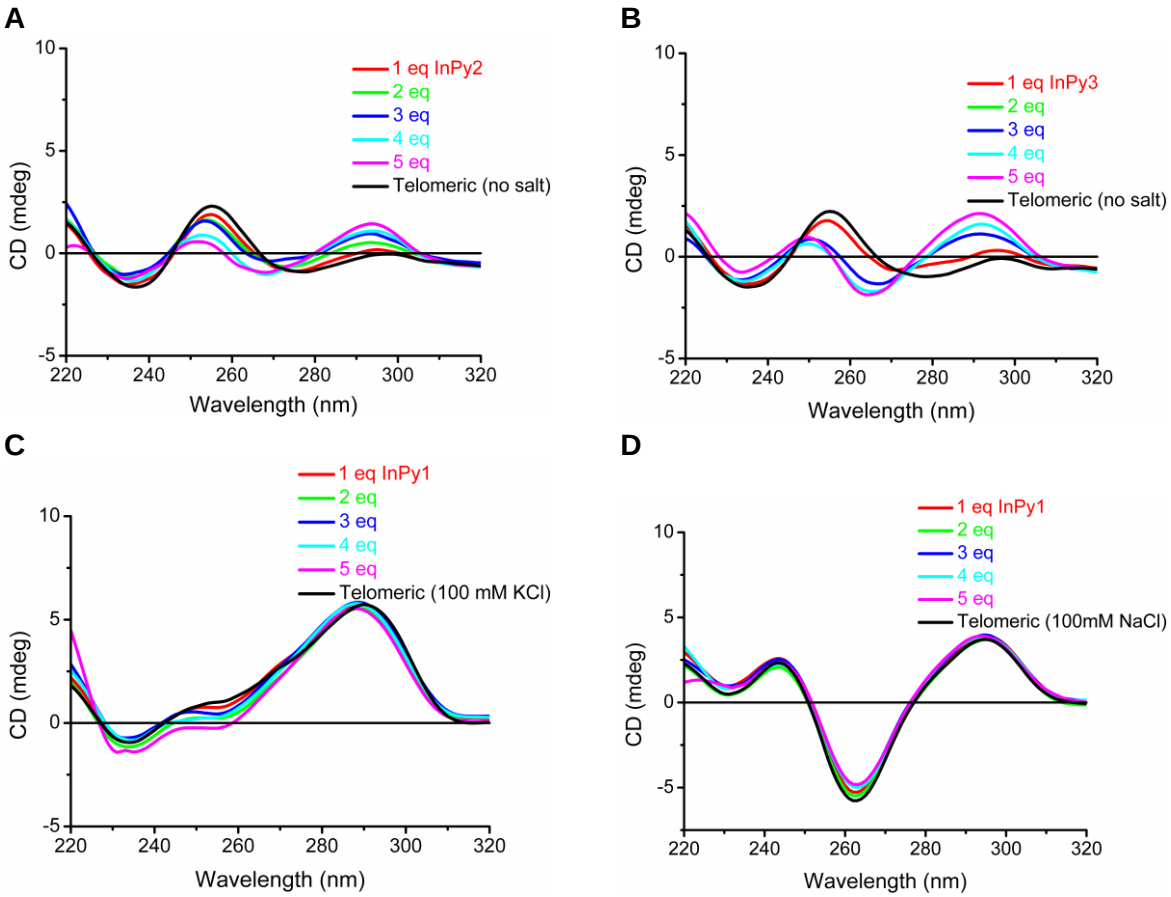

Figure S1. CD titration spectra of telomeric DNA (12.5 µM in 50 mM Tris pH 7.2) with ligands in the absence/presence of added monovalent metal ions. (A) Telomeric DNA with **InPy2**; (B) Telomeric DNA with **InPy3**; (C) Telomeric DNA in 100 mM KCl with **InPy1**; (D) Telomeric DNA in 100 mM NaCl with **InPy1**.

CD spectra for ligands with *c-myc* DNA in the absence/presence of K^+ ions

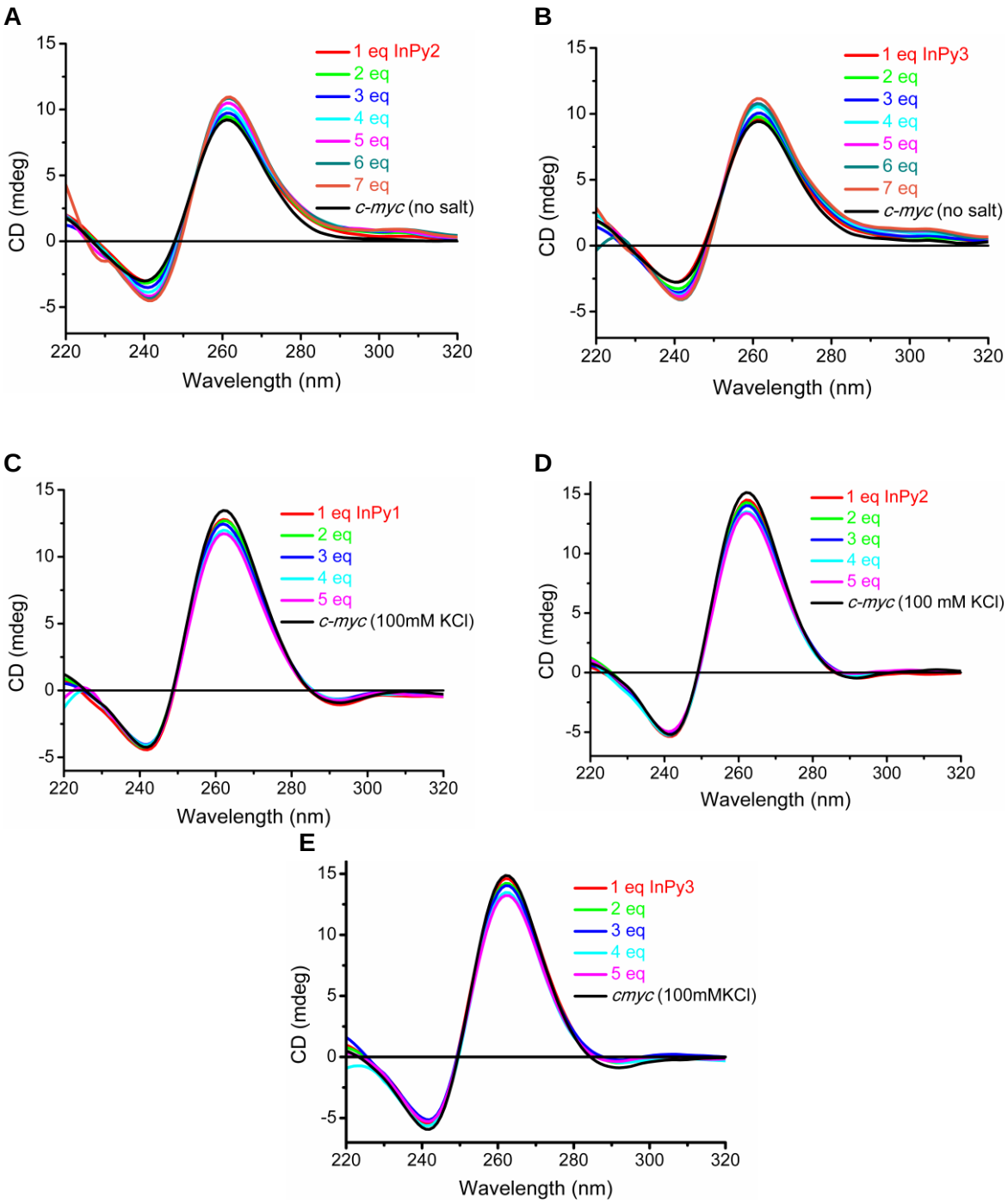

Figure S2. CD titration spectra of *c-myc* DNA (12.5 µM and 50 mM Tris pH 7.2) with ligands in the absence/presence of added monovalent metal ions. (A) *c-myc* DNA with **InPy2**; (B) *c-myc* DNA with **InPy3**; (C) *c-myc* DNA in 100 mM KCl with **InPy1**; (D) *c-myc* DNA in 100 mM KCl with **InPy2**; (E) *c-myc* DNA in 100 mM KCl with **InPy3**.

CD spectra for ligands with *c-kit1* DNA in the absence/presence of K^+ ions

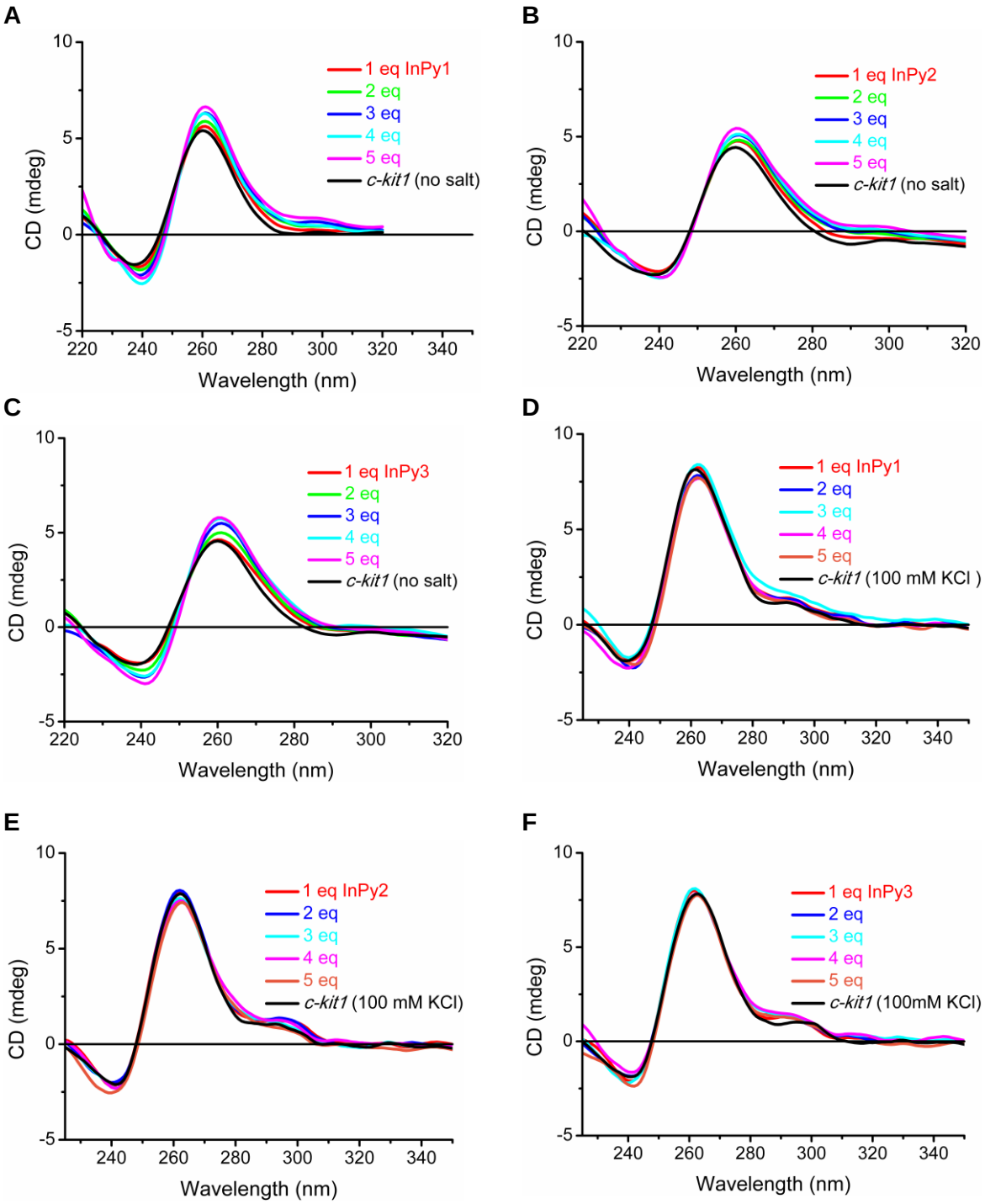

Figure S3. CD titration spectra of *c-kit1* DNA (12.5 μM in 50 mM Tris pH 7.2) with ligands in the absence/presence of added monovalent metal ions. (A) *c-kit1* DNA with **InPy1**; (B) *c-kit1* DNA with **InPy2**; (C) *c-kit1* DNA with **InPy3**; (D) *c-kit1* DNA in 100 mM KCl with **InPy1**; (E) *c-kit1* DNA in 100 mM KCl with **InPy2**; (F) *c-kit1* DNA in 100 mM KCl with **InPy3**.

CD melting curves for *c-kit1*, duplex and telomeric DNAs

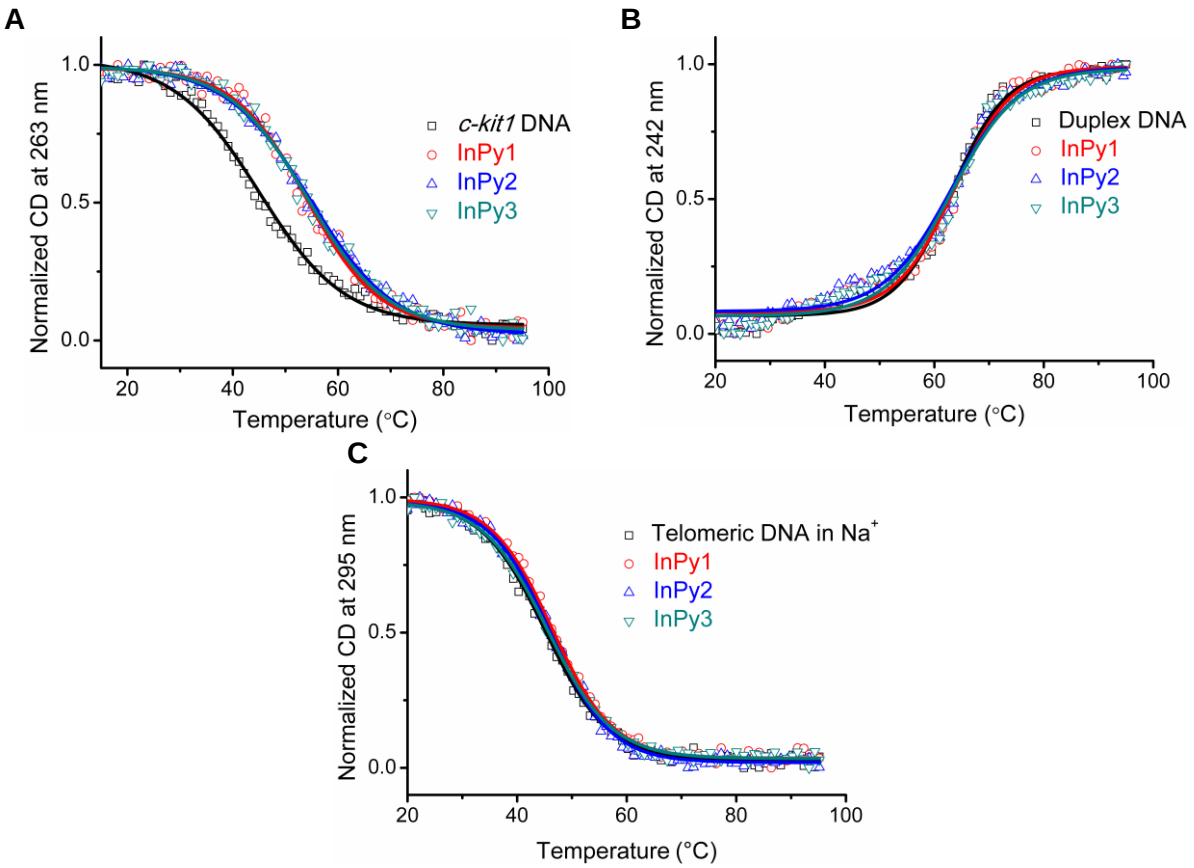

Figure S4. CD melting curves of *c-kit1*, duplex (in 10 mM KCl, 90 mM LiCl and 10 mM lithium cacodylate buffer pH 7.2) and telomeric DNAs in the absence and presence of 5 equivalents of ligands. (A) *c-kit1* (10 µM); (B) Duplex DNA (15 µM); (C) Telomeric DNA (10 µM in 10mM NaCl, 90 mM LiCl and 10mM sodium cacodylate)

Fluorimetric titration curves for InPy1 with telomeric and duplex DNAs

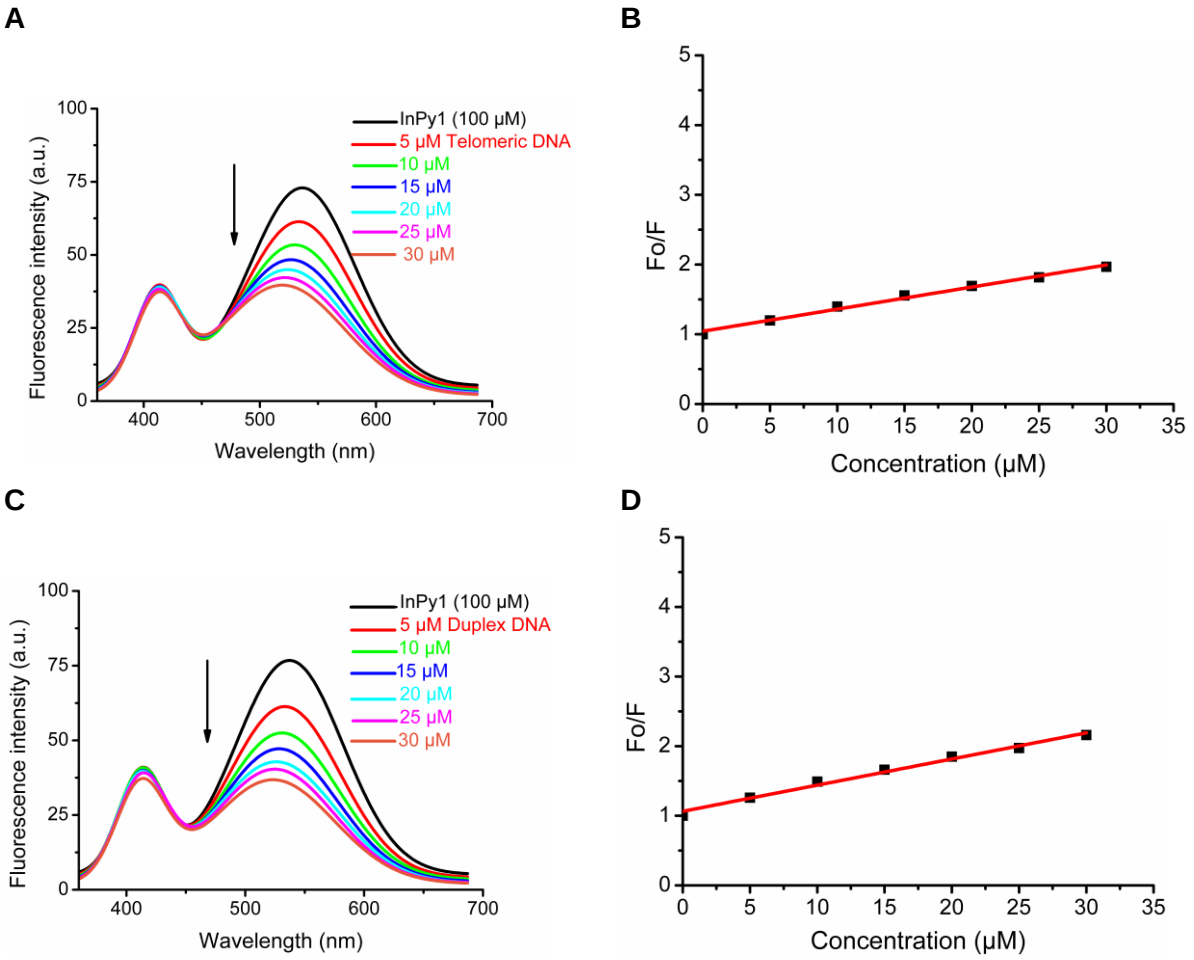

Figure S5. Fluorescence quenching curves and Stern-Volmer plots for **InPy1** (100 μM in 100 mM KCl and 10 mM lithium cacodylate buffer pH 7.2) with increasing concentration of telomeric and duplex DNAs (0-30 μM pre-annealed under identical salt and buffer conditions). (A) Quenching curve for **InPy1** with telomeric DNA; (B) Stern-Volmer plot for **InPy1** with telomeric DNA; (C) Quenching curve for **InPy1** with duplex DNA; (D) Stern-Volmer plot for **InPy1** with duplex DNA. Binding constant values were reported as the average with standard deviation of 3 independent experiments.

Fluorimetric titration curves for InPy2 with *c-myc*, telomeric and duplex DNAs

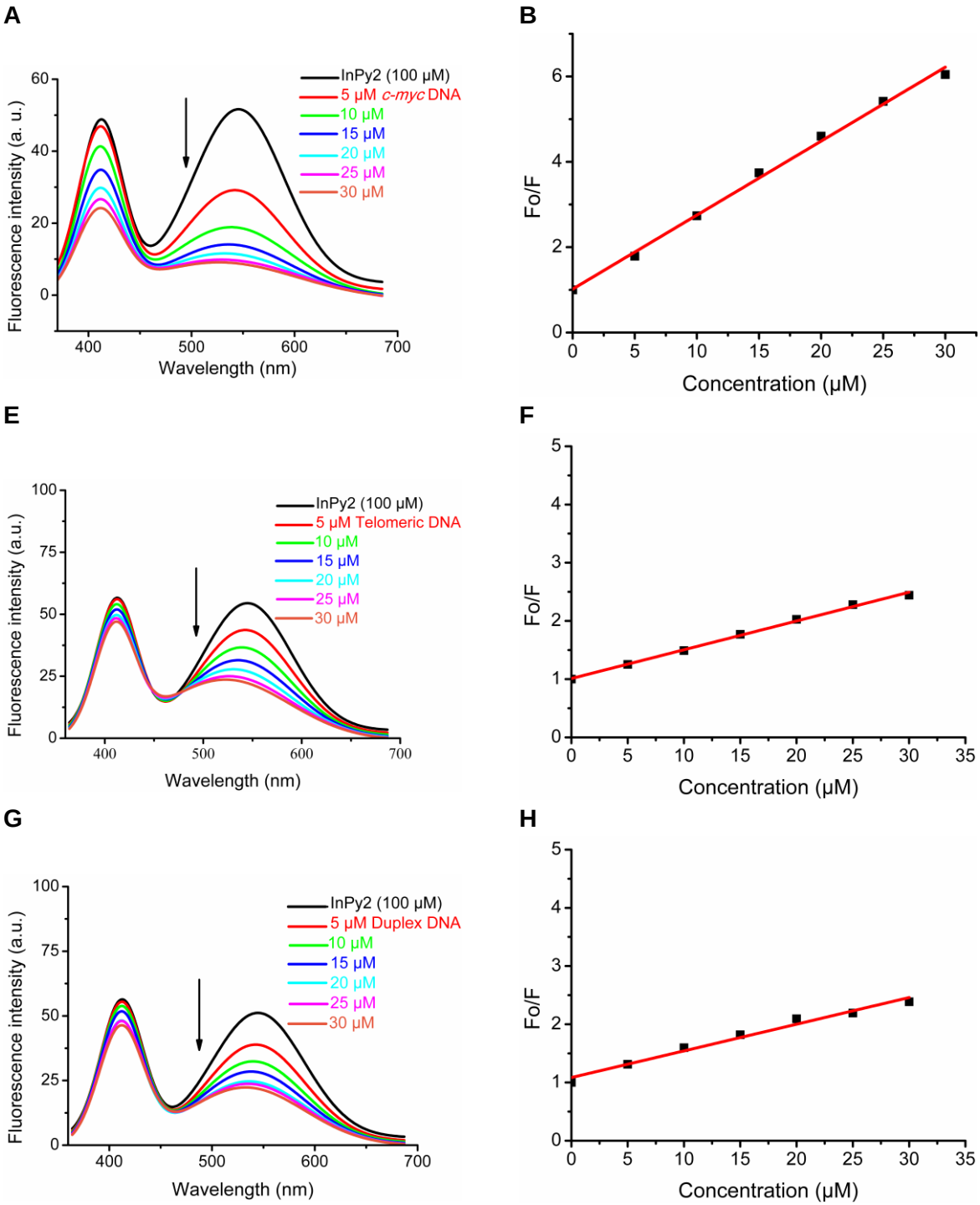

Figure S6. Fluorescence quenching curves and Stern-Volmer plots for **InPy2** (100 μM in 100 mM KCl and 10 mM Lithium cacodylate buffer pH 7.2) with increasing concentration of *c-myc*, telomeric and duplex DNAs (0-30 μM pre-anealed under identical salt and buffer conditions). (A) Quenching curve for **InPy2** with *c-myc* DNA; (B) Stern-Volmer plot for **InPy2** with *c-myc* DNA; (C) Quenching curve for **InPy2** with telomeric DNA; (D) Stern-Volmer plot for **InPy2** with telomeric DNA (E) Quenching curve for **InPy2** with duplex DNA; (F) Stern-Volmer plot for **InPy2** with duplex DNA. Binding constant values were reported as the average with standard deviation of 3 independent experiments.

Job plot analysis for InPy1 with *c-myc* quadruplex DNA

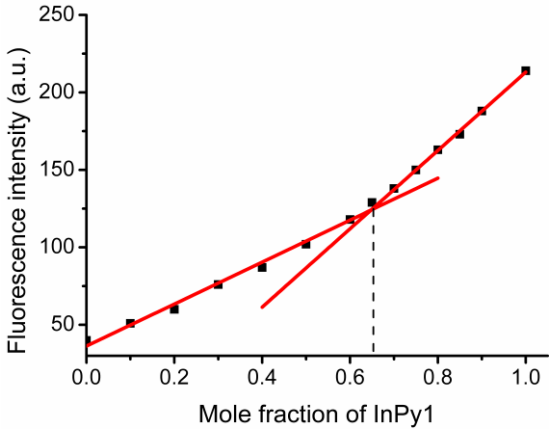

Figure S7. Job plot analysis of fluorescence for **InPy1** with *c-myc* quadruplex DNA. Total molar concentration (ligand + DNA) was kept constant at 5 µM. Excitation wavelength used was 350 nm. An inflection point at 0.65 indicates stoichiometry of ~ 2:1 for ligand:DNA interaction.

PAGE and IC_{50} plots of *Taq* DNA polymerase stop assay

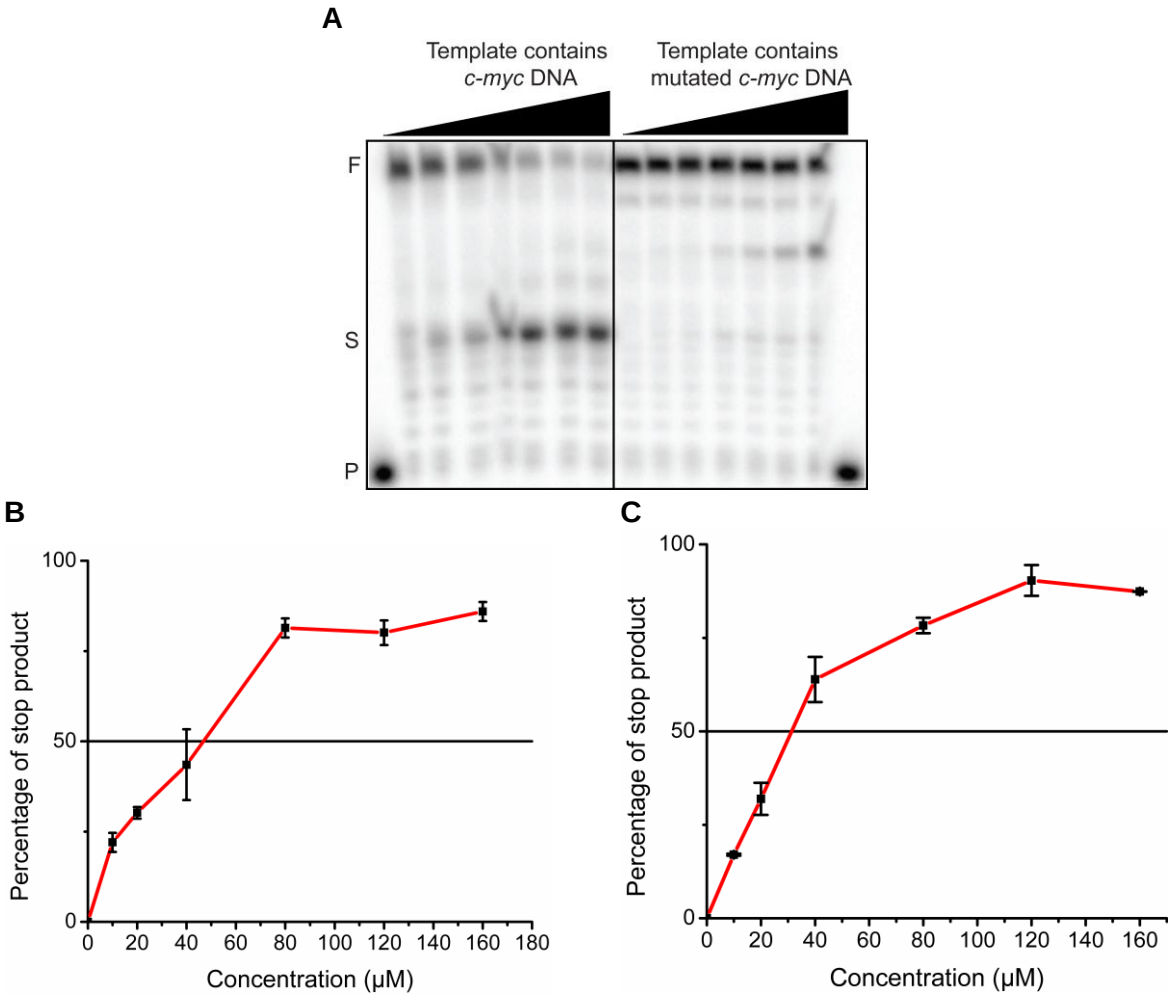

Figure S8. Denaturing PAGE (15%, 7M urea) and plots of *Taq* polymerase stop products versus ligand concentration: Normalized percentage of stop products in each lane was plotted against concentration of ligand. (A) Denaturing PAGE for the *Taq* DNA polymerase stop assay with template containing *c-myc* and mutated *c-myc* DNA with increasing concentration of **InPy2** (0-160 μM); (B) Plot of *Taq* polymerase stop products versus **InPy1** concentration (0-160 μM); (C) Plot of *Taq* polymerase stop products versus **InPy2** concentration (0-160 μM). Primer extension reaction at 50°C. Conditions: 100 nM template, 50 nM primer, 0.2 mM dNTPs, 5 mM KCl in *Taq* polymerase buffer (50 mM Tris, 0.5 mM DTT, 0.1 mM EDTA, 5 mM $MgCl_2$, 5mM KCl for *c-myc* template). Error bar represents standard deviation for 3 independent experiments.

Energy optimized structure of InPy1 at HF/6-31G* level

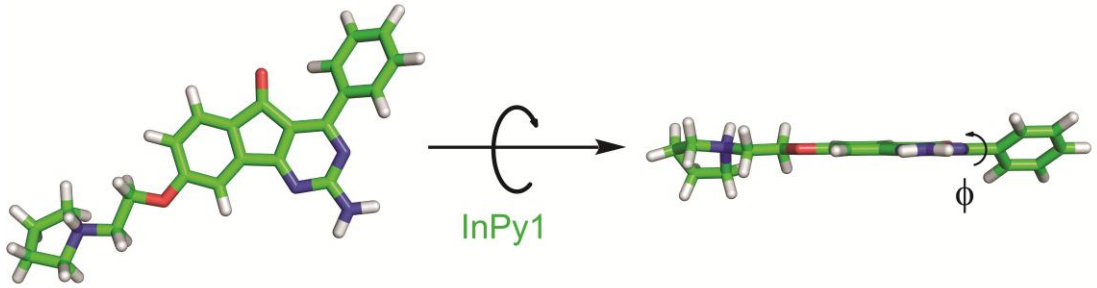

Figure S9. Energy optimized structure of InPy1 using HF/6-31G* level in Gaussian 09. InPy1 in axial (left) and side (right) view shown in figure, and phi (ϕ) is the angle between indenopyrimidine and benzene ring. RESP charges were calculated at same level in Gaussian 09. Figures were rendered using PyMOL.

Docked structure of InPy1 with *c-myc* DNA

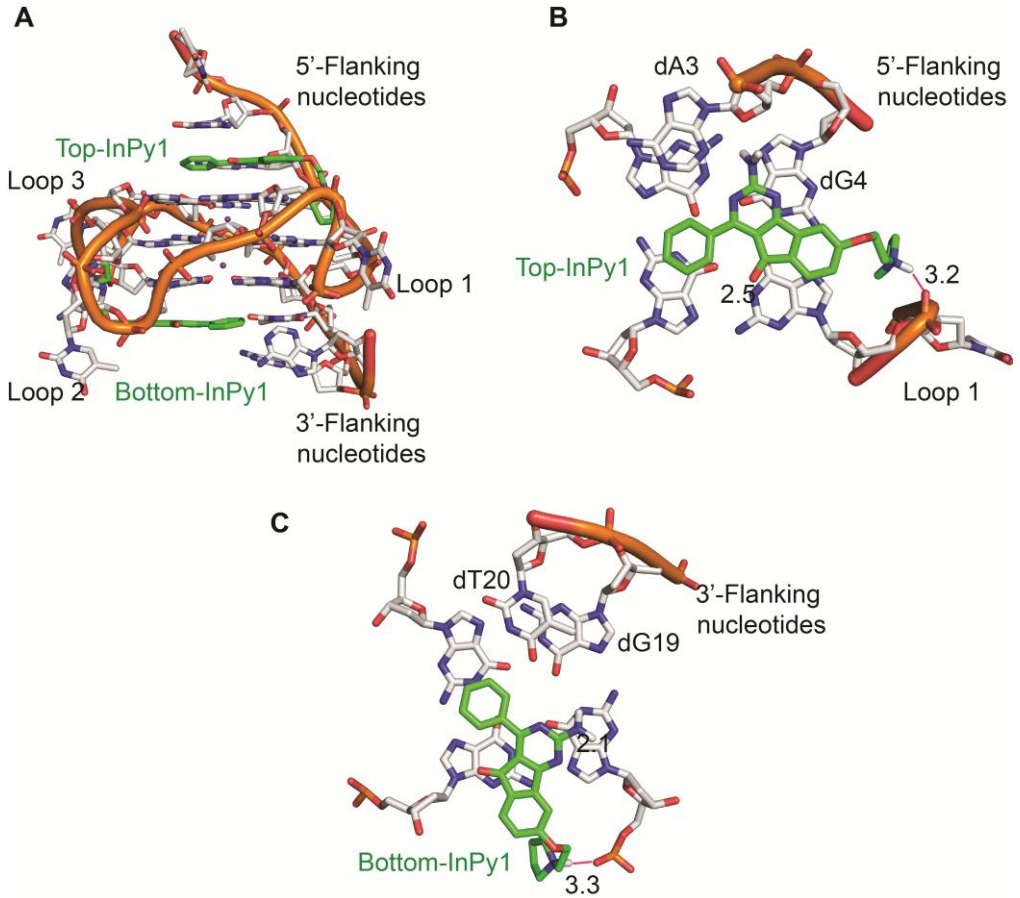

Figure S10. Docked structure of **InPy1** with *c-myc* G-quadruplex DNA using Autodock 4.2. (A) **InPy1** and *c-myc* G-quadruplex DNA (2:1) stacks at both top and bottom G-quartet of G-quadruplex; (B) **InPy1** and top quartet (axial view), (C) **InPy1** and bottom quartet (axial view) showing electrostatic interaction with phosphate backbone of the G-quadruplex DNA. Figures were rendered using PyMOL.

Docked structure of InPy1 with *c-kit1* DNA

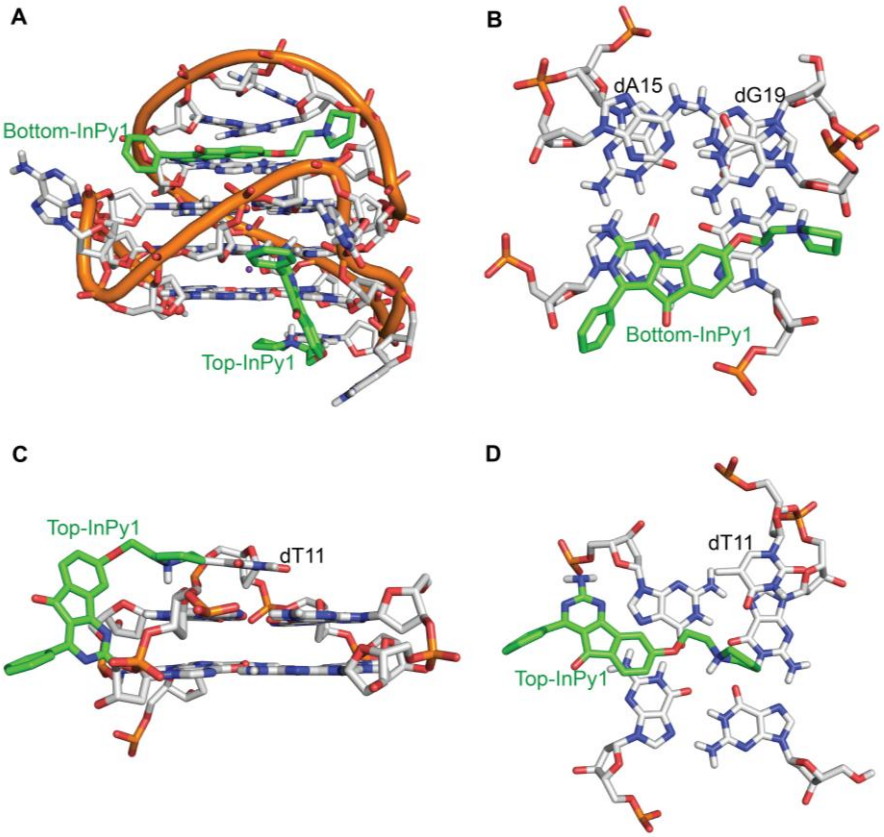

Figure S11. Docked structure of **InPy1** with *c-kit1* G-quadruplex DNA using Autodock Vina (O. Trott, A. J. Olson, *J. Comput. Chem.* **2010**, *31*, 455−461). (A) **InPy1** and *c-kit1* G-quadruplex DNA (2:1) stacks at bottom G-quartet of G-quadruplex and binds to the groove near the top quartet; (B) **InPy1** and bottom quartet (top view), (C) **InPy1** and top quartet (side view), (D) **InPy1** and top quartet after 350 ps of equilibration using AMBER12 (top view). Figures were rendered using PyMOL.

Time dependent RMSD graphs of *c-myc* DNA and InPy1

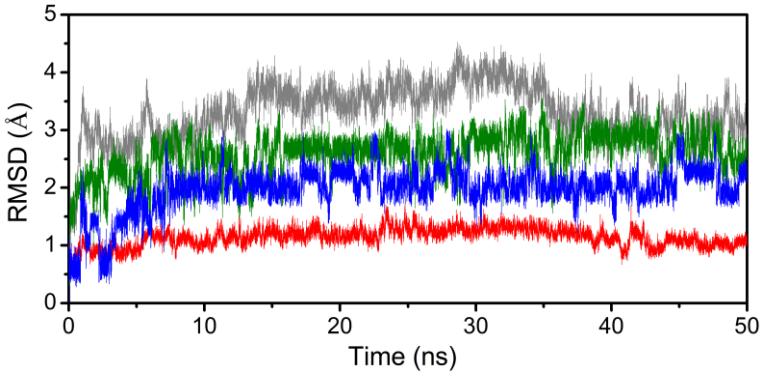

Figure S12. Time dependent root mean square deviation graph (RMSD) of *c-myc* G-quadruplex DNA complexed with InPy1. RMSD of backbone (grey), G-quartet (red), top-InPy1 (blue) and bottom-InPy1 (green) were plotted against time. RMSDs were calculated at each ps during 50 ns of MD simulations using ptraj module in AMBER 12.

Time dependent RMSD graphs of *c-kit1* DNA and InPy1

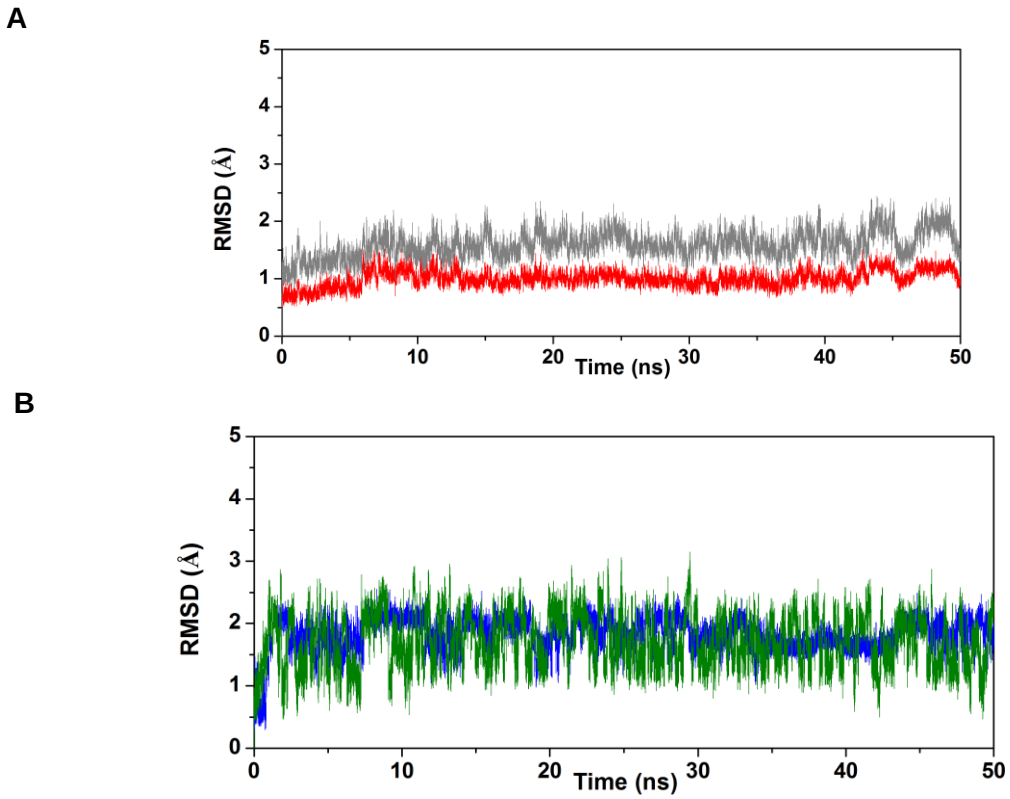

Figure S13. Time dependent root mean square deviation graph (RMSD) of *c-kit1* G-quadruplex DNA complexed with InPy1. (A) RMSD of backbone (grey) and G-quartet (red), (B) RMSD of top-InPy1 (green) and bottom-InPy1 (blue) were plotted against time. RMSDs were calculated at each ps during 50 ns of MD simulations using ptraj module in AMBER 12.

Binding free energy components of *c-myc* DNA and InPy1

MD Simulations (50 ns)	*c-myc* G-quadruplex DNA (PDB entry: 2L7V)		
	Dual	**Top-InPy1**	**Bottom-InPy1**
ΔE_{ELEC}	−889.19 ± 27.09	−442.59 ± 18.68	−456.60 ± 25.91
ΔE_{VDW}	−88.96 ± 7.18	−44.15 ± 2.8	−44.81 ± 7.20
$\Delta E_{MM}(\Delta E_{Elec}+\Delta E_{VDW})$	−988.15 ± 31.01	−486.75 ± 19.34	−501.41 ± 31.68
ΔPB_{np}	−10.02 ± 0.60	−5.02 ± 0.20	−5.00 ± 0.61
ΔPB_{cal}	923.67 ± 27.48	453.02 ± 18.03	470.62 ± 27.37
ΔPB_{solv} ($\Delta PB_{np}+\Delta PB_{cal}$)	913.65 ± 27.10	448.00 ± 17.92	465.61 ± 26.85
$\Delta G_{PB}(\Delta E_{mm}+\Delta PB_{solv})$	**−74.51 ± 7.38**	**−38.75 ± 3.72**	**−35.80 ± 6.98**
ΔGB_{np}	−10.02 ± 0.60	−5.02 ± 0.20	−5.00 ± 0.61
ΔGB_{cal}	910.53 ± 26.16	445.90 ± 17.02	464.75 ± 25.89
ΔGB_{solv} ($\Delta GB_{np}+\Delta GB_{cal}$)	900.51 ± 25.08	440.88 ± 16.92	459.75 ± 25.38
$\Delta G_{GB}(\Delta E_{MM}+\Delta GB_{solv})$	−87.64 ± 7.30	−45.87 ± 3.52	−41.66 ± 7.51
ΔS_{TRANS}	−13.64 ± 0.00	−13.07 ± 0.01	−13.07 ± 0.01
ΔS_{ROTA}	−12.90 ± 0.04	−10.97 ± 0.01	−10.99 ± 0.02
ΔS_{VIBR}	−2.85 ± 0.74	8.60 ± 1.80	6.41 ± 1.19
$T\Delta S$	−29.39 ± 0.78	−15.46 ± 1.80	−15.65 ± 1.18
ΔG ($\Delta G_{PB} - T\Delta S$)	**−45.12 ± 7.43**	**−22.56 ± 4.13**	**−19.15 ± 7.07**

Table S1. Binding free energy components of *c-myc* G-quadruplex DNA with **InPy1** calculated from last 15 ns of 50 ns MD simulations. The molecular mechanical energy calculations are calculated using MM/PB-GBSA and entropy calculations are carried using nmode in AMBER 12. ΔE_{ELEC} is the electrostatic interaction, ΔE_{VDW} is the Vander Waals contribution, ΔE_{MM} is the total molecular-mechanical energy (ΔE_{ELEC} + ΔE_{VDW} + ΔE_{ini} (zero for all)). ΔG_{np} is the nonpolar contribution to the solvation energy. ΔG_{PB} and ΔG_{GB} are the electrostatic contribution to the solvation energy calculated; ΔPB_{solv} and ΔGB_{solv} are the total solvation energy. $T\Delta S$ is solute entropic contribution, where T = temperature and ΔS is the sum of translational, rotational, and vibrational entropies. ΔG is the estimated binding free energy with solute entropic contribution ($\Delta G_{GB} - T\Delta S$). All the values are reported in kcal mol^{-1}.

Binding free energy components of *c-kit1* DNA and InPy1

MD Simulations (50 ns)	*c-kit1* G-quadruplex DNA (PDB entry: 2O3M)		
	Dual	**Top-InPy1**	**Bottom-InPy1**
ΔE_{ELEC}	−847.33 ± 25.43	−357. 39 ± 16.69	−489.93 ± 16.61
ΔE_{VDW}	−76.78 ± 4.02	−31.63 ± 3.15	−45.15 ± 2.15
$\Delta E_{MM}(\Delta E_{Elec}+\Delta E_{VDW})$	−924.11 ± 27.21	−389.02 ± 18.41	−535.08 ± 17.05
ΔPB_{np}	−8.29 ± 0.35	−3.48 ± 0.32	−4.81 ± 0.13
ΔPB_{cal}	863.24 ± 24.69	362.47 ± 17.48	500.58 ± 14.73
ΔPB_{solv} ($\Delta PB_{np}+\Delta PB_{cal}$)	854.94 ± 24.46	358.98 ± 17.22	495.77 ± 14.69
$\Delta G_{PB}(\Delta E_{mm}+\Delta PB_{solv})$	**−69.17 ± 5.15**	**−30.05 ± 3.22**	**−39.31 ± 3.85**
ΔGB_{np}	−8.29 ± 0.35	−3.48 ± 0.32	−4.81 ± 0.13
ΔGB_{cal}	852.28 ± 23.11	359.50 ± 16.57	492.96 ± 13.64
ΔGB_{solv} ($\Delta GB_{np}+\Delta GB_{cal}$)	843.99 ± 22.88	356.01 ± 16.32	488.15 ± 13.60
$\Delta G_{GB}(\Delta E_{MM}+\Delta GB_{solv})$	−80.12 ± 5.80	−33.01 ± 3.32	−46.93 ± 4.27
ΔS_{TRANS}	−13.64 ± 0.01	−13.07 ± 0.00	−13.07 ± 0.00
ΔS_{ROTA}	−12.79 ± 0.02	−10.95 ± 0.02	−10.99 ± 0.02
ΔS_{VIBR}	−1.59 ± 0.12	7.78 ± 0.13	6.71 ± 0.04
$T\Delta S$	−28.02 ± 0.15	−16.24 ± 0.15	−17.35 ± 0.06
ΔG ($\Delta G_{PB} - T\Delta S$)	**−43.78 ± 5.15**	**−13.81 ± 3.22**	**−22.96 ± 3.85**

Table S2. Binding free energy components of *c-kit1* G-quadruplex DNA with **InPy1** calculated from last 15 ns of 50 ns MD simulations. The molecular mechanical energy calculations are calculated using MM/PB-GBSA and entropy calculations are carried using nmode in AMBER 12. ΔE_{ELEC} is the electrostatic interaction, ΔE_{VDW} is the Vander Waals contribution, ΔE_{MM} is the total molecular-mechanical energy ($\Delta E_{ELEC} + \Delta E_{VDW} + \Delta E_{ini}$ (zero for all)). ΔG_{np} is the nonpolar contribution to the solvation energy. ΔG_{PB} and ΔG_{GB} are the electrostatic contribution to the solvation energy calculated; ΔPB_{solv} and ΔGB_{solv} are the total solvation energy. $T\Delta S$ is solute entropic contribution, where T = temperature and ΔS is the sum of translational, rotational, and vibrational entropies. ΔG is the estimated binding free energy with solute entropic contribution ($\Delta G_{GB} - T\Delta S$). All the values are reported in kcal mol^{-1}.

Average RMSDs of G-Quadruplex DNA and InPy1 complex

Heavy atoms of DNA and ligand	*c-myc* G-quadruplex DNA	*c-kit1* G-quadruplex DNA
G-quartet	1.14 ± 0.16	1.00 ± 0.15
DNA backbone	3.31 ± 0.48	1.60 ± 0.23
InPy1	2.60 ± 0.36 (top-**Inpy1**)	1.71 ± 0.43 (top-**Inpy1**)
	1.97 ± 0.38 (bottom-**InPy1**)	1.83 ± 0.27 (bottom-**InPy1**)

Table S3. Average RMSD values (Å) of the heavy atoms in the backbone, G-quartet and **InPy1**-G-quadruplex DNA complex. RMSDs were calculated at each ps from 50 ns of MD simulations using ptraj module in AMBER 12. Errors indicate the standard deviation.

Hoogsteen hydrogen bond occupancy in G-quartet during MD simulations

G-quartet	Percentage occupancy (*c-myc)*	Percentage occupancy (*c-kit1)*
Top quartet	99.74%	99.59%
Middle quartet	99.13%	96.29%
Bottom quartet	99.64%	99.29%

Table S4. The percentage occupancy of Hoogsteen hydrogen bond between the guanine bases present in each G-quartet. The occupancy was calculated at each ps during 50 ns of MD simulations using ptraj module in AMBER 12.

^{1}H NMR of compound 6

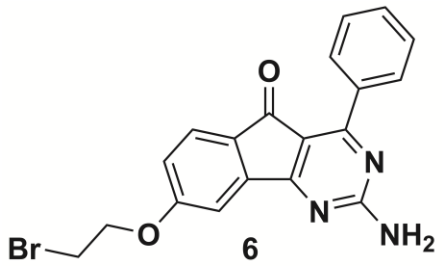

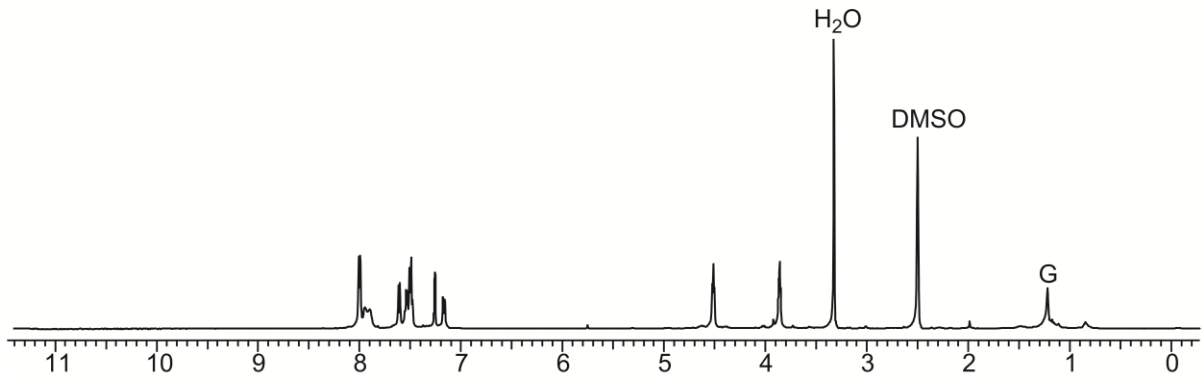

^{13}C NMR of compound 6

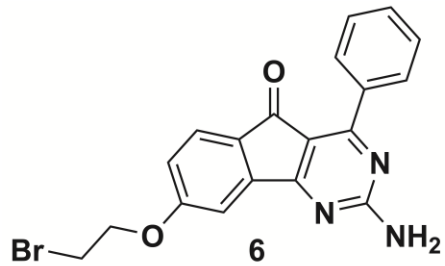

^{1}H NMR of compound 7

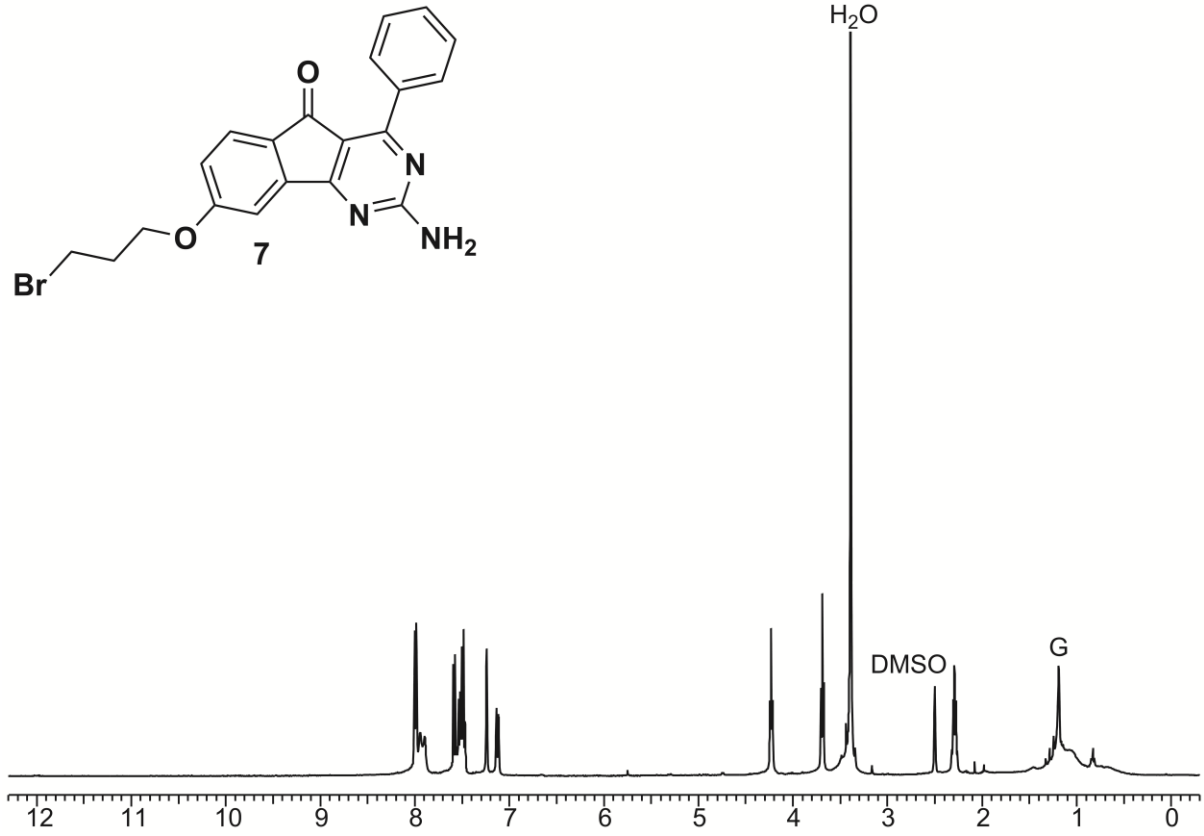

^{13}C NMR of compound 7

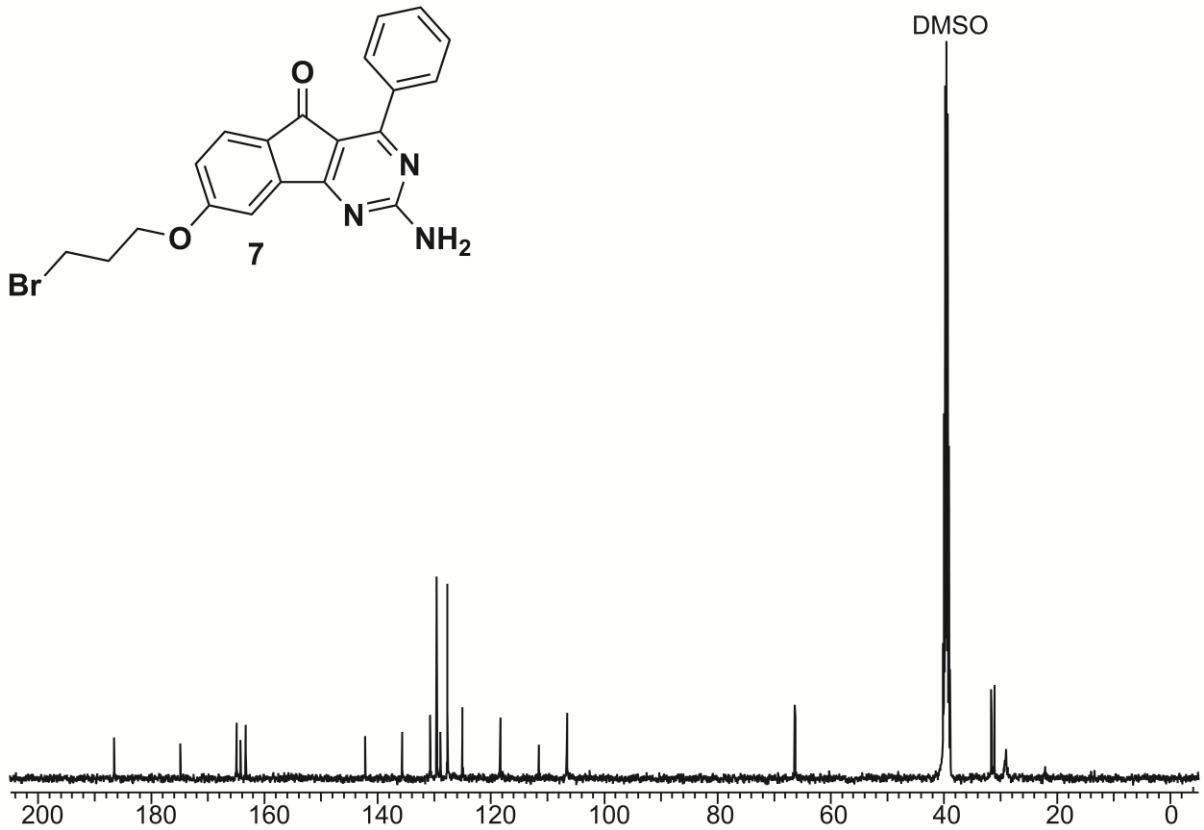

^{1}H NMR of compound InPy1

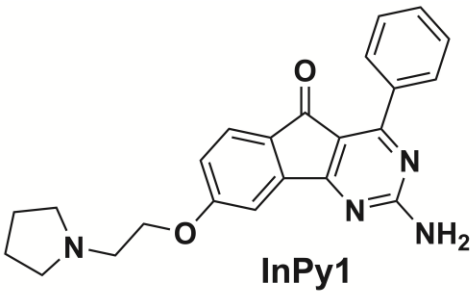

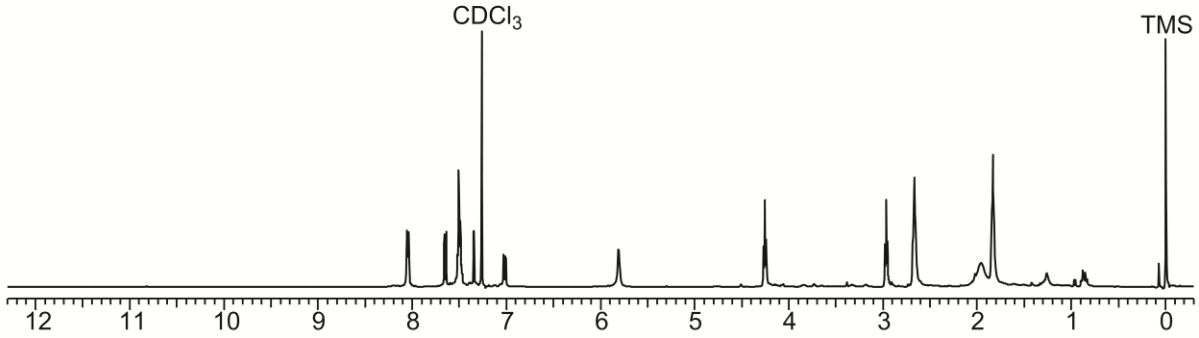

^{13}C NMR of compound InPy1

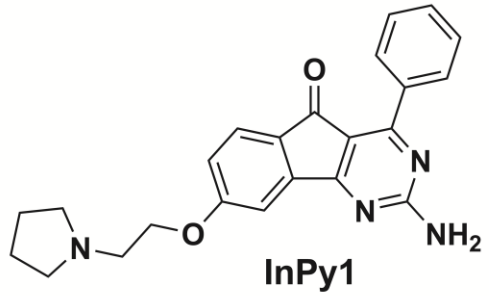

^{1}H NMR of compound InPy2

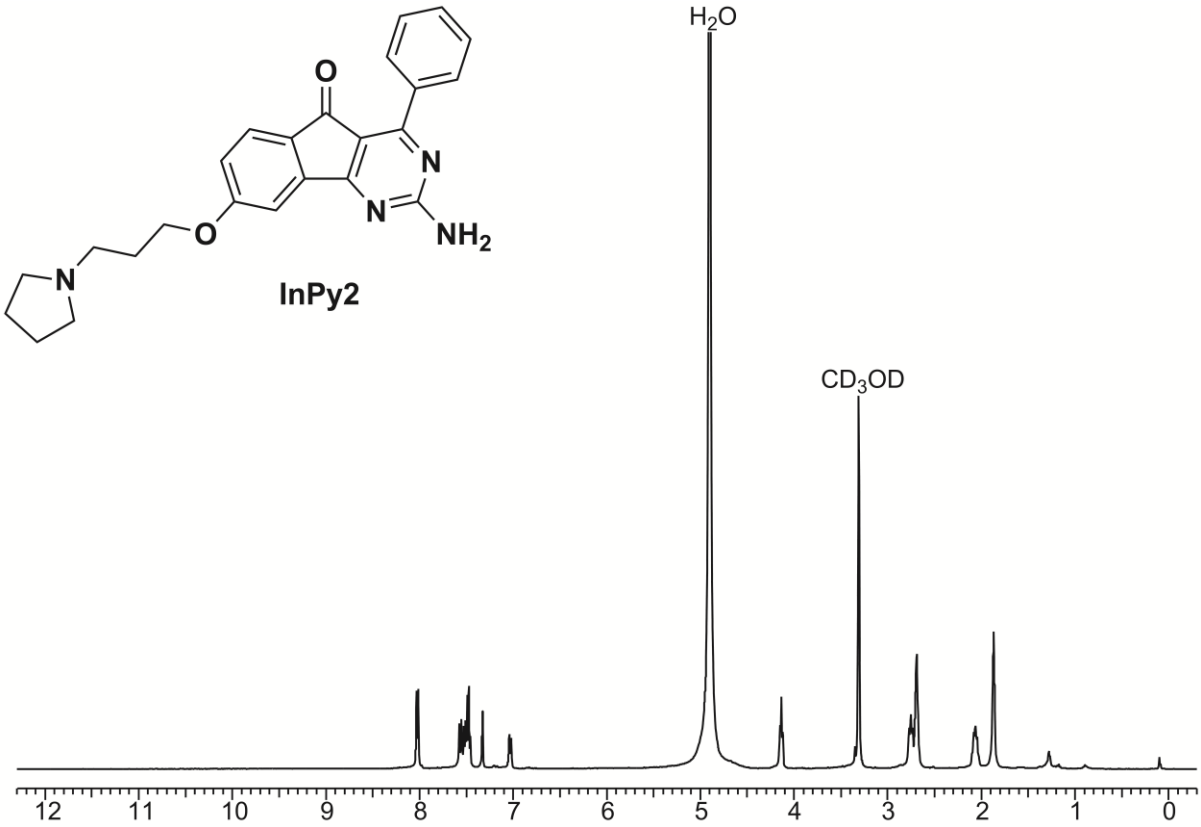

^{13}C NMR of compound InPy2

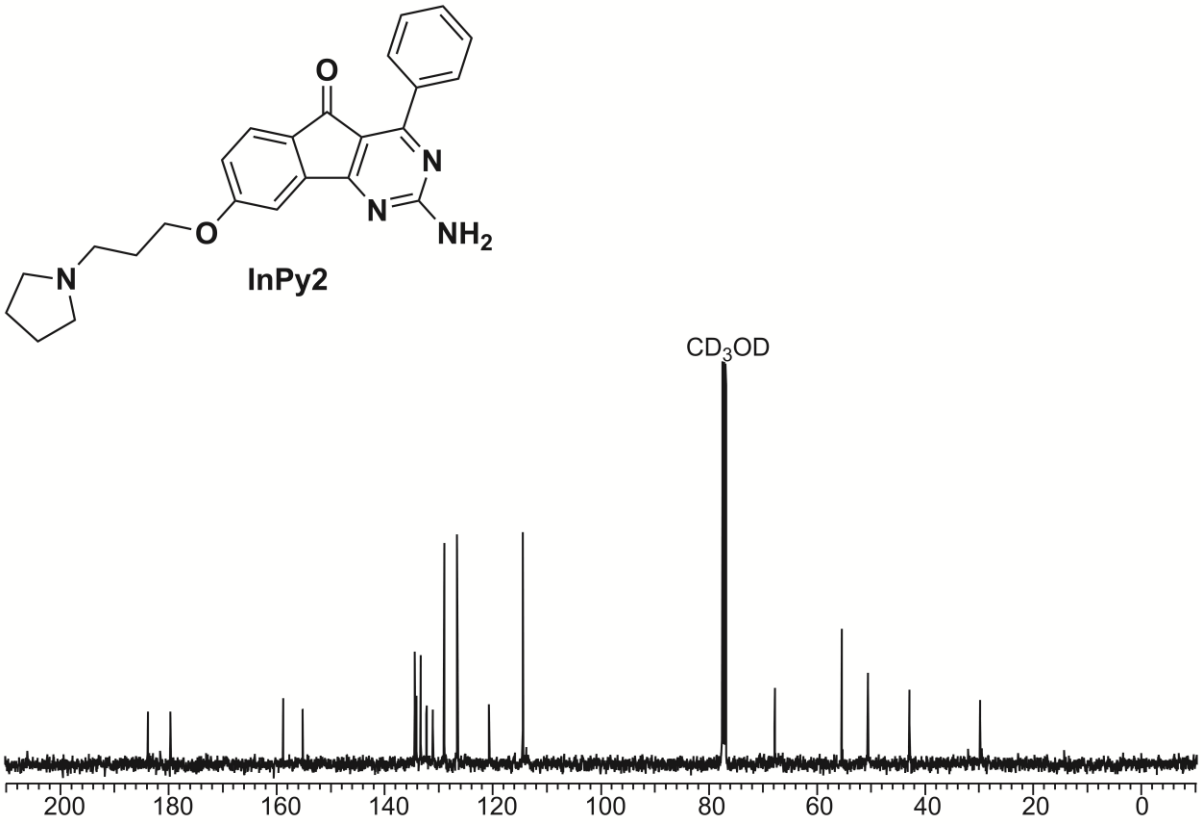

^{1}H NMR of compound InPy3

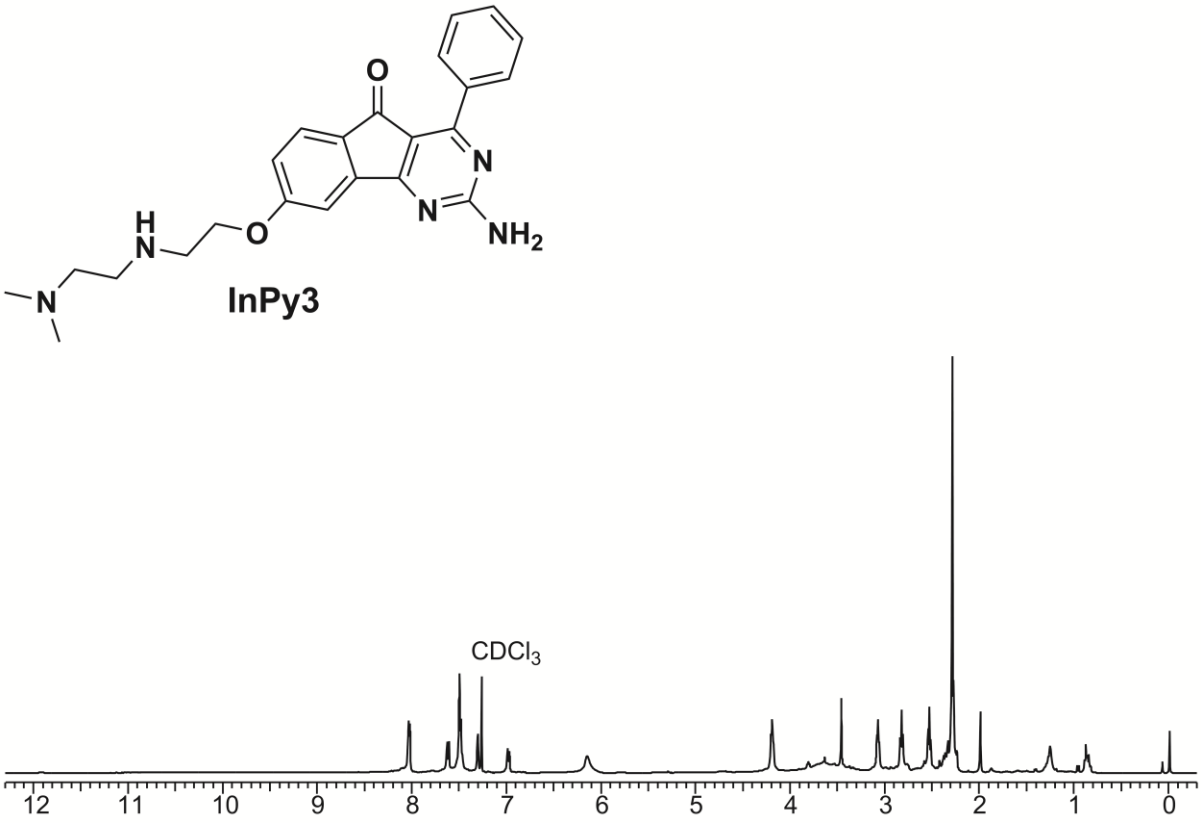

^{13}C NMR of compound InPy3